Physical volcanology of the Pavagadh rhyolites, northern Deccan Traps: Stratigraphic, structural, and textural record of explosive and effusive eruptions

Janisar M. Sheikh[1] (*Email: janisar.sk@gmail.com*), Hetu Sheth[2], Anmol Naik[2], Tanmay Keluskar[2]

[1]Centre of Advanced Study in Geology, Institute of Science, Banaras Hindu University, Varanasi 221005, India

[2]Department of Earth Sciences, Indian Institute of Technology Bombay, Mumbai 400076, India

1. Introduction

The origin of silicic rocks found in continental flood basalt (CFB) provinces is a topic of considerable petrogenetic interest, and whether these rocks represent explosive or effusive volcanism is another interesting and important question since it has implications for the environmental impact of the flood volcanism. This is because explosive eruptions can inject ash and magmatic gases to much greater heights in the atmosphere than effusive eruptions, with correspondingly significantly wider distribution. In the present work, rhyolites at and around Mount Pavagadh, representing one such locality of silicic rocks in the northern part of the Deccan Traps CFB province (Fig. 1) were investigated in terms of stratigraphy, outcrop structures and textures to understand the nature and style of their eruption from modern volcanological perspectives.

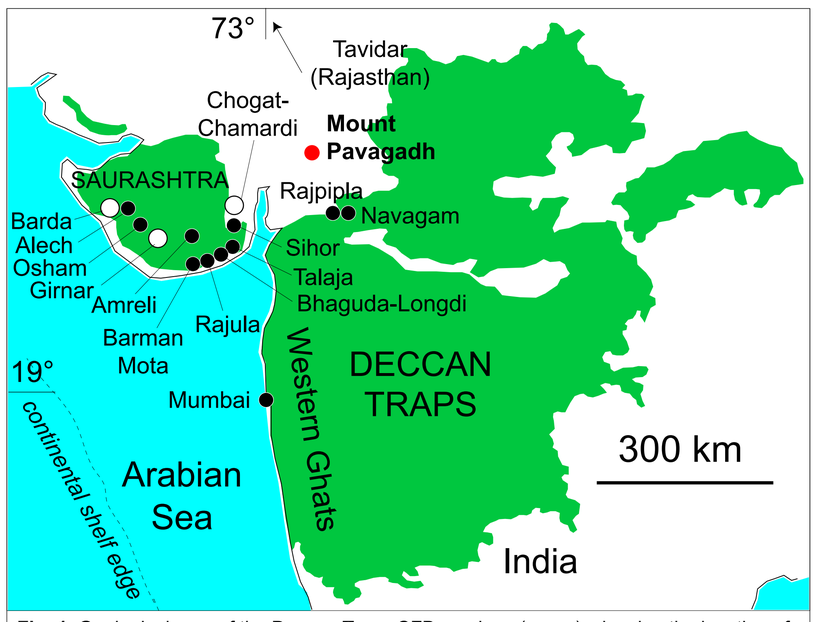

Fig. 1. Geological map of the Deccan Traps CFB province (green), showing the location of Mount Pavagadh (red circle). Black and whilte circles denote notable locations of silicic rocks in the province.

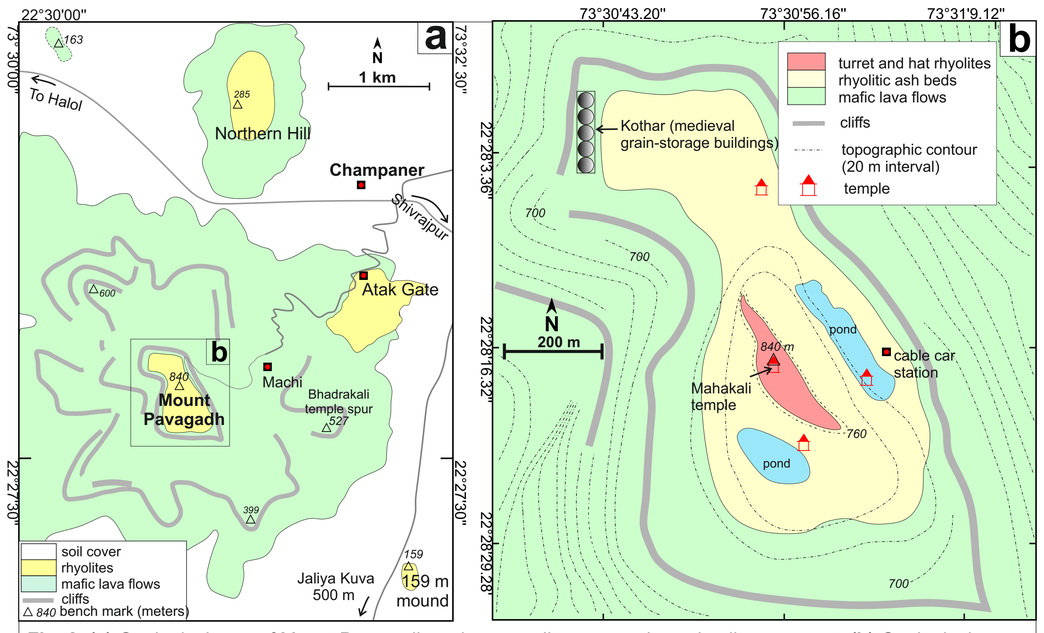

Fig. 2. (a) Geological map of Mount Pavagadh and surrounding areas where rhyolites crop out. **(b)** Geological map of the 748 m basalt plateau of Mount Pavagadh

2. Geological Setting and Volcanic Stratigraphy

Mount Pavagadh, rising ~700 m above the surrounding plains of Precambrian igneous and metamorphic basement rocks and Quaternary alluvium, is an outlier of the Malwa plateau forming the northern part of the Deccan Traps CFB province (Figs. 1, 2). The Pavagadh sequence is dominated by horizontal mafic lava flows (e.g., basalt, picrite, ankaramite, alkali olivine basalt, hawaiite, mugearite), which are overlain by rhyolites at the top of the main mountain, Atak Gate, 159 m mound and northern hill (Figs. 2a). The rhyolites on the main Pavagadh mountain top constitute a 47 m thick "ash sequence" containing tens of non-welded, ash beds (Figs. 2b, 3, 4). The ash sequence is overlain by a 50 m thick "turret sequence" of dark grey lava flow with basal and upper breccias, and a local basal vitrophyre. The turret is covered at the top by "hat-sequence" of an ignimbrite with a basal vitrophyre (Figs. 2b, 3, 4). Rhyolite boulders at Atak Gate, 159 m mound and northern hill are either blocks eroded from turret rhyolites, or lava flows from separate eruptionsm (Fig. 2a).

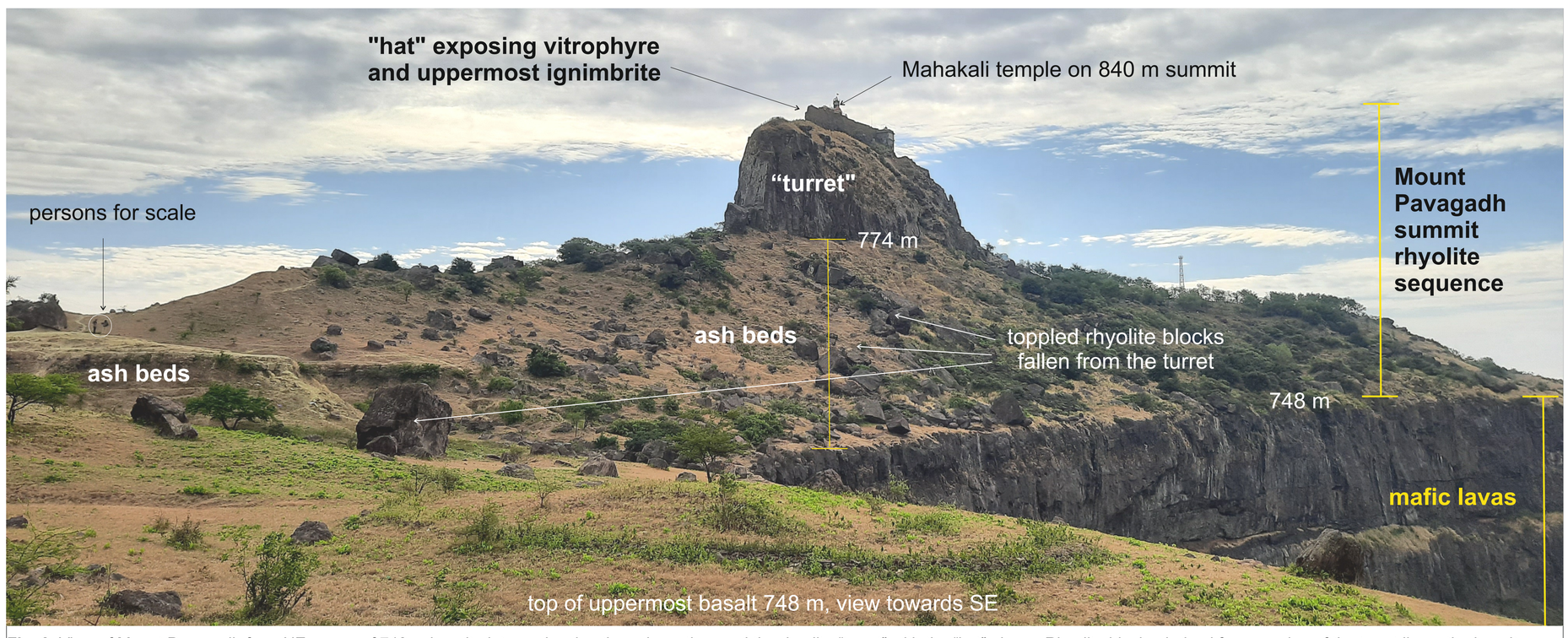

Fig. 3. View of Mount Pavagadh from NE corner of 748 m basalt plateau showing the ash section, and the rhyolite "turret" with the "hat" above. Rhyolite blocks derived from erosion of the turret lie on the basalt plateau and on the slopes of the ash section; a few are indicated.

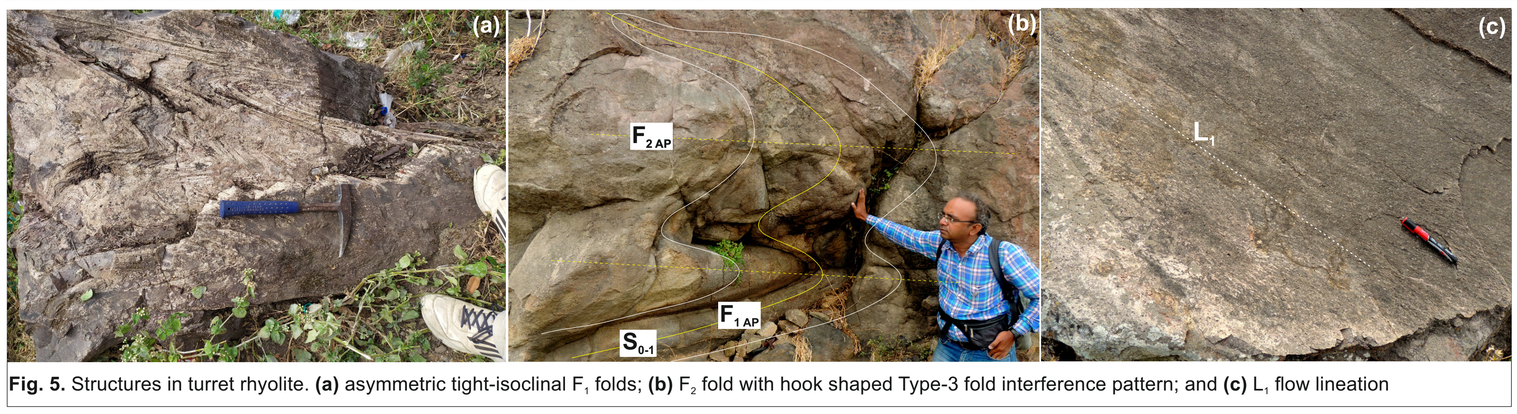

Fig. 5. Structures in turret rhyolite. **(a)** asymmetric tight-isoclinal F_1 folds; **(b)** F_2 fold with hook shaped Type-3 fold interference pattern; and **(c)** L_1 flow lineation

4. Textures

Lapilli tuff at the base of ash sequence comprises large fibrous pumice fragments, while the ash beds are rich in glass and pumice with a few crystals (Figs. 6a,b). Turret rhyolite show fine microcrystalline quartzo-feldspathic matrix and phenocrysts of plagioclase, olivine and Fe-Ti oxide (Fig. 6c). Turret breccia shows fragmental texture with angular fragments of flow banded/glassy rhyolite (Fig. 5d), while the basal vitrophyre shows glassy groundmass, phenocrysts of plagioclase, clinopyroxene, olivine and Fe-Ti oxide, but no vitroclasts (Fig. 6g). Vitrophyre and ignimbrite forming the hat sequence show excellent vitroclastic texture, both consist of abundant platy, curved, or Y-shaped shards, and flattened and folded fibrous pumice fiamme (Fig. 6e,f). Rhyolites at Atak Gate, 159 m mound show microcrystalline matrix of skeletal to anhedral feldspar and quartz, and phenocrysts of orthoclase and oligoclase; while northern hill rhyolite shows microscopic flow bands warping around feldspar phenocrysts (Fig. 6h).

5. Physical Volcanological Interpretations

The glass and pumice-rich ash beds in the Pavagadh upper rhyolite sequence are interpreted as Plinian fallout deposits from very distant sources, each of the ash beds represents the fallout ash associated with an ignimbrite eruption. The turret rhyolite with basal and upper breccias, a local basal vitrophyre, and rheomorphic deformation features is an uncommon sheet-like lava flow of flood rhyolite and probably had a significant minimum original volume of 5 km^3. An ignimbrite with a basal vitrophyre overlies the lava flow and forms the summit of the mountain, and is also from a distal source. The upper rhyolites thus represent alternating explosive-effusive-explosive eruptions. Massive deposits of ignimbrite corresponding the Pavagadh rhyolites are required, these are nowhere to be found nearby, but they may be the ignimbrites found at many locations in Saurashtra. Rhyolites that crop out at lower elevations on the mountain and in surrounding areas are probably also lavas, though distinct from the turret rhyolite lava in many features and therefore independently erupted. Geochemical and geochronological work on the Pavagadh rhyolites is needed, in the stratigraphic and volcanological context provided here, to understand their petrogenesis and potential relationship with the Cretaceous/Palaeogene (K/Pg) boundary mass extinction.

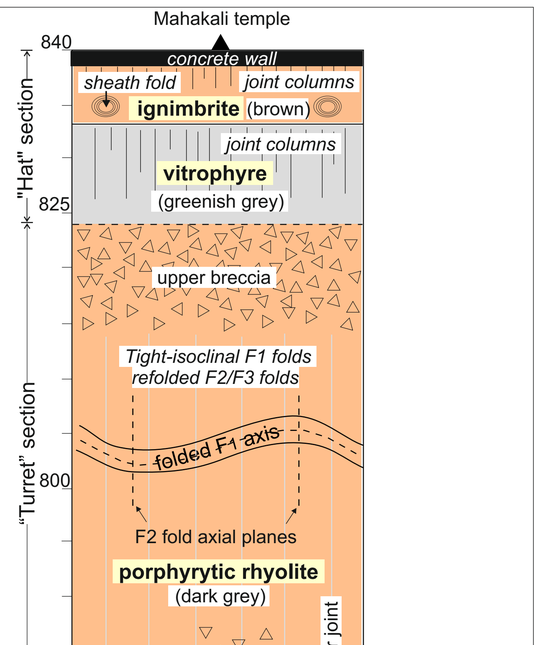

Fig. 4. Stratigraphic log of the Mount Pavagadh upper rhyolites showing some of the main physical features of the units

3. Structures

Turret rhyolite, it's eroded blocks toppled over ash beds and rhyolite boulders at Atak Gate, 159 m mound and northern hill, all show spectacular rheomorphic structures in the form of flow banding and flow folding. Common folds are symmetric to asymmetric tight-isoclinal F_1 folds (Fig. 5a), F_2 folds with hook-shaped Type-3 fold interference patterns (Fig. 5b), F_1 sheath folds refolded by gentle F_2 folds. L_1 flow lineations are observed on fold surface (Fig. 5c). Columnar jointing is observed in turret well as in hat sequence.

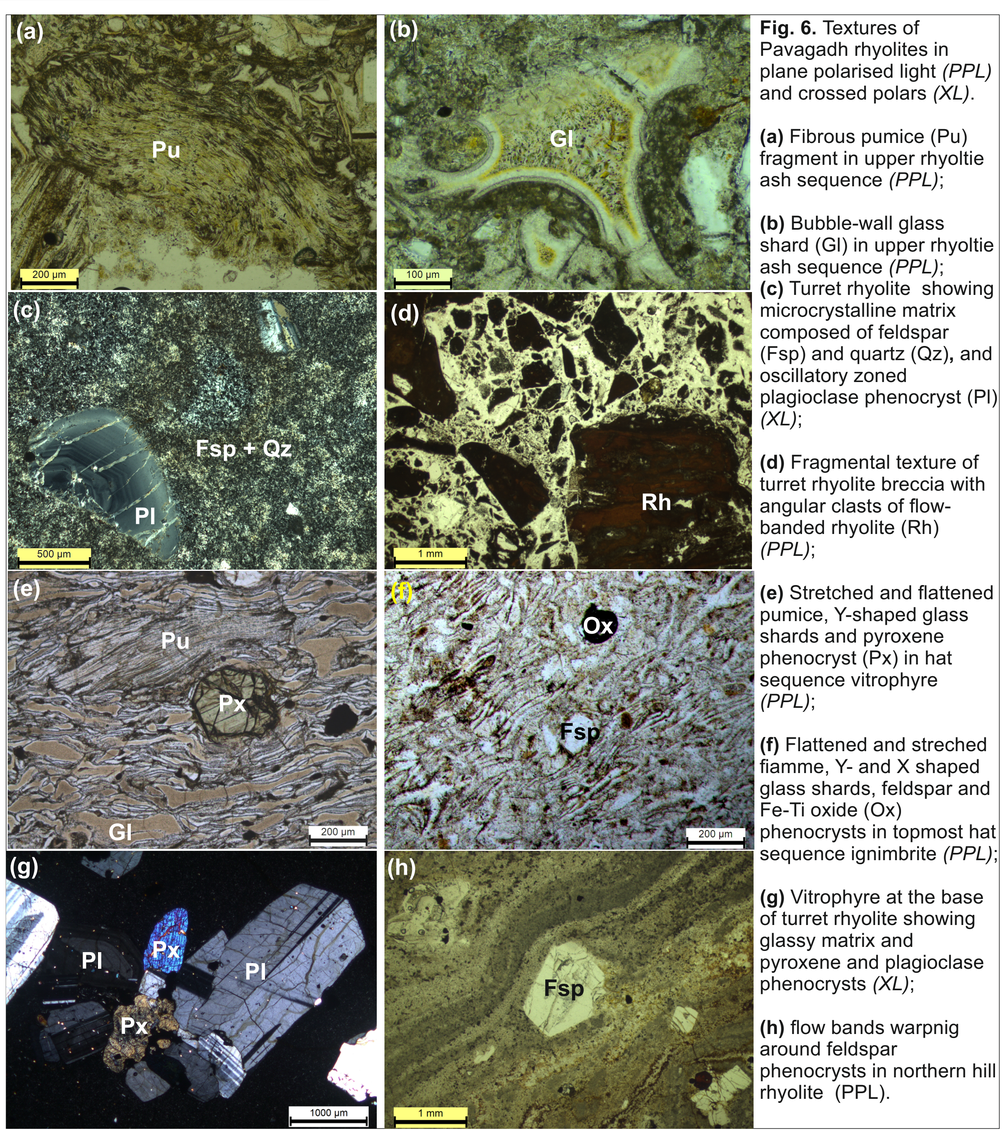

Fig. 6. Textures of Pavagadh rhyolites in plane polarised light *(PPL)* and crossed polars *(XL)*.

(a) Fibrous pumice (Pu) fragment in upper rhyoltie ash sequence *(PPL)*;

(b) Bubble-wall glass shard (Gl) in upper rhyoltie ash sequence *(PPL)*;

(c) Turret rhyolite showing microcrystalline matrix composed of feldspar (Fsp) and quartz (Qz), and oscillatory zoned plagioclase phenocryst (Pl) *(XL)*;

(d) Fragmental texture of turret rhyolite breccia with angular clasts of flow-banded rhyolite (Rh) *(PPL)*;

(e) Stretched and flattened pumice, Y-shaped glass shards and pyroxene phenocryst (Px) in hat sequence vitrophyre *(PPL)*;

(f) Flattened and streched fiamme, Y- and X shaped glass shards, feldspar and Fe-Ti oxide (Ox) phenocrysts in topmost hat sequence ignimbrite *(PPL)*;

(g) Vitrophyre at the base of turret rhyolite showing glassy matrix and pyroxene and plagioclase phenocrysts *(XL)*;

(h) flow bands warpnig around feldspar phenocrysts in northern hill rhyolite (PPL).

Aknowledgements: *JMS is supported by a Malaviya Postdoctoral Fellowship of Banaras Hindu University (IoE Scheme, Ref. No. IoE/MPDF/2020-21/14)*

CHEMICAL WEATHERING RATE OF A SMALL WESTERN GHAT RIVER, SOUTHWESTERN INDIA

V.N AMRISH, K. BALAKRISHNA, H.N UDAYA SHANKARA, ARUN KUMAR AND NISHITHA D'SOUZA

Introduction: Quantification of chemical weathering of silicate rocks and associated atmospheric carbon dioxide consumption rates (CCR) is significant as it provides a better understanding of long-term climate change.

Methodology:

- Twenty-four water samples were collected in monsoon 2018 (n = 9), post-monsoon season 2018 (n = 8), and pre-monsoon 2019.
- Major ions using Ion-Chromatography.
- Basic physico-chemical parameters - measured in-situ.
- Bicarbonates - auto titrator and silica by UV-spectrometer.

Study area:

- The river originates -Western Ghats and debouches into the Arabian Sea.
- The upstream -mainly gneissic
- The downstream - gneiss, quartzite, schist, and greywacke.

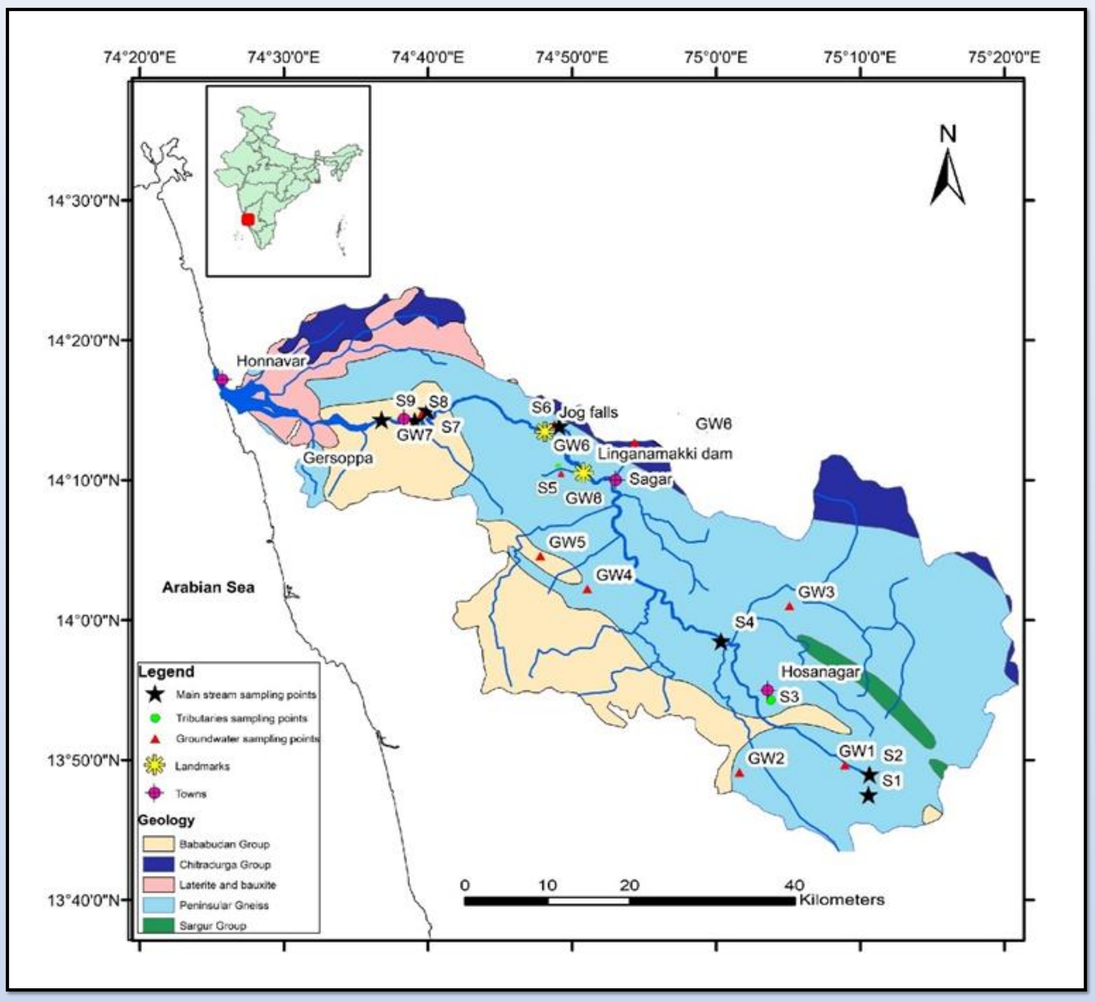

Results and discussions:

- Silicate Weathering Rate (SWR) for the watershed - 27 $t.km^{-2}.y^{-1}$
- Compared- east- flowing- Krishna and Bhima, the SWR of Sharavati river is 2-3 times higher.
- The samples -fall close to the silicate end member on the Ca/Mg vs Mg/Na plot.
- The presence of clay mineral- kaolinite in the catchment indicates intense rainfall, hot and humid climate, and high silicate weathering rates.
- These factors and associated river discharge control the major ion chemistry in the Sharavati river.
- Carbon dioxide consumption rate is 3.9 x 10^5 $mol.km^{-2}.y^{-1}$.

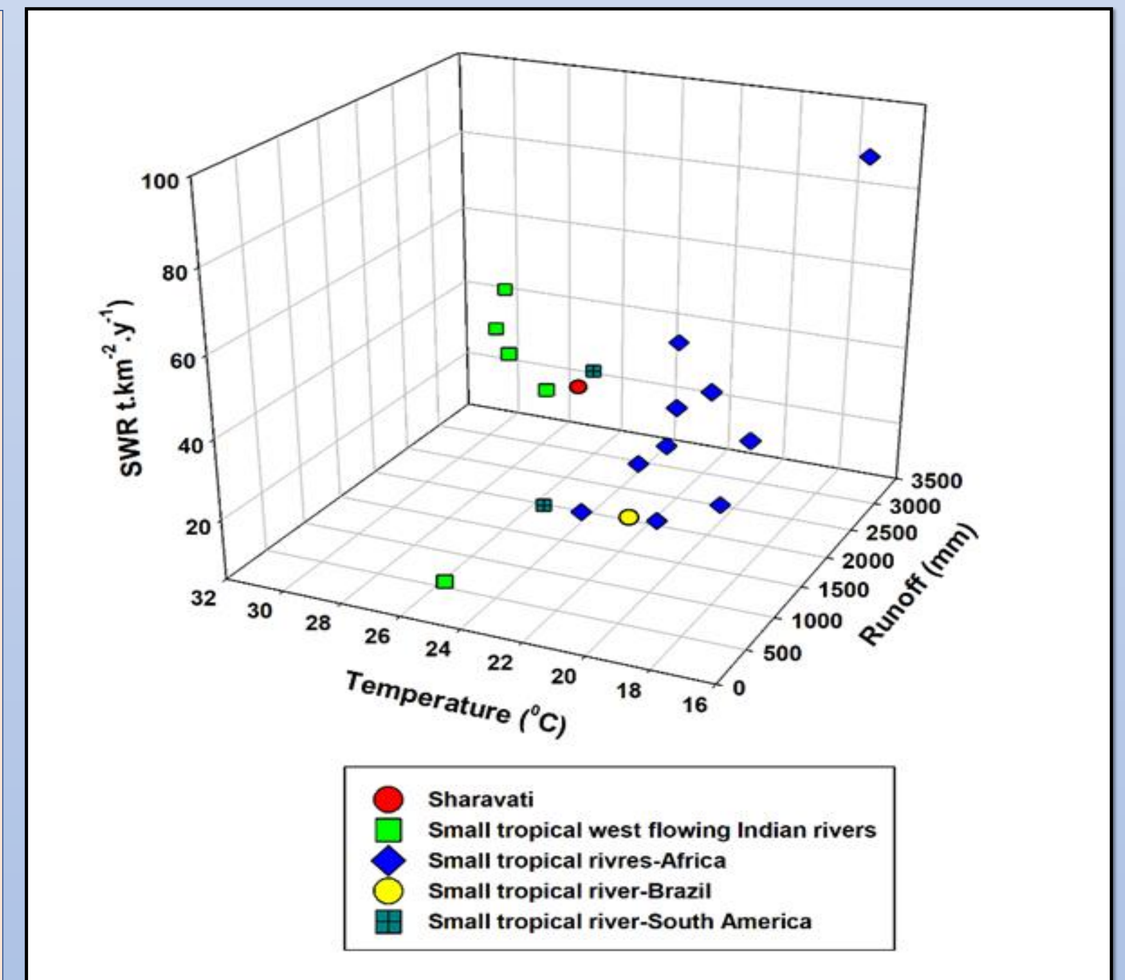

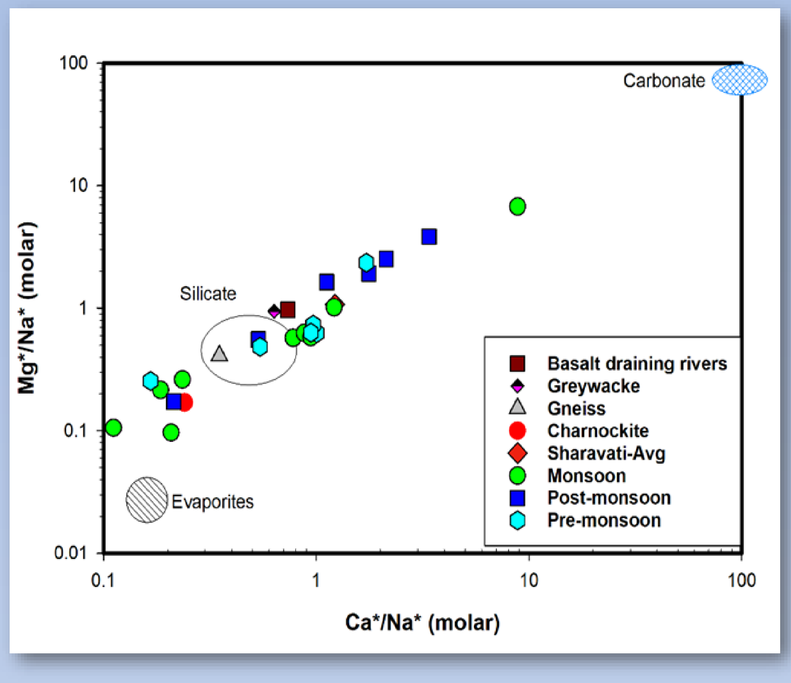

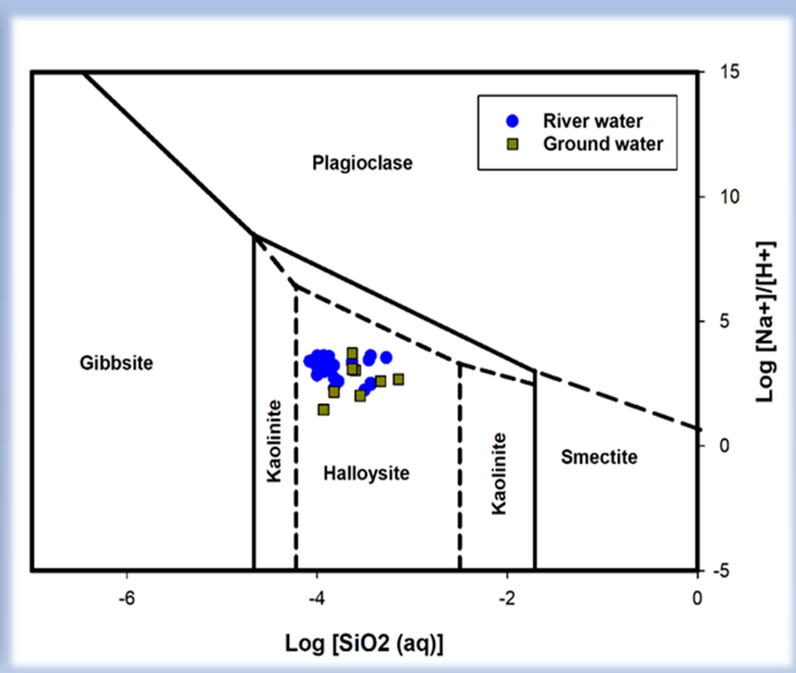

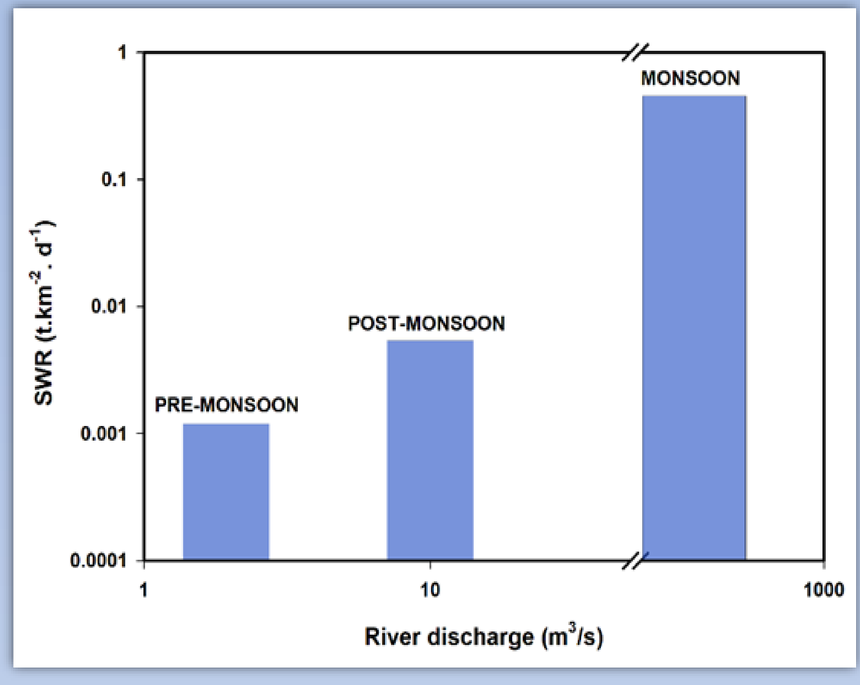

Conclusions: CCR is 3.9 times higher than the global average on account of the peculiarity of the terrain. From the study, it can be concluded that all the small (< 4500 km^2) tropical watersheds show control of rainfall irrespective of different lithologies and associated runoff on SWR.

Drastic change in sediment provenance during the Permian-Triassic transition: An insight from Sr-Nd isotopic study of Guryul Ravine section, India

Anirban Mandal[1,*], Gyana Ranjan Tripathy[1], Satyabarta Das[2], Santosh Kumar Rai[2], Suraj K Parcha[2]and Rakesh Chandra[3]
[1]Department of Earth and Climate Science, Indian Institute of Science Education and Research (IISER), Pune, India
[2]Wadia Institute of Himalayan Geology, 33 GMS road, Dehradun-248001, India
[3]Department of Geology, University of Ladakh, Leh-194101, India
(*Presenting Author: anirban.mandal@students.iiserpune.ac.in)

Late Permian Mass extinction

The Late Permian mass extinction, the largest bio-crisis event in the Earth's history, was responsible for wiping out about 90% of marine and 75% of terrestrial species.

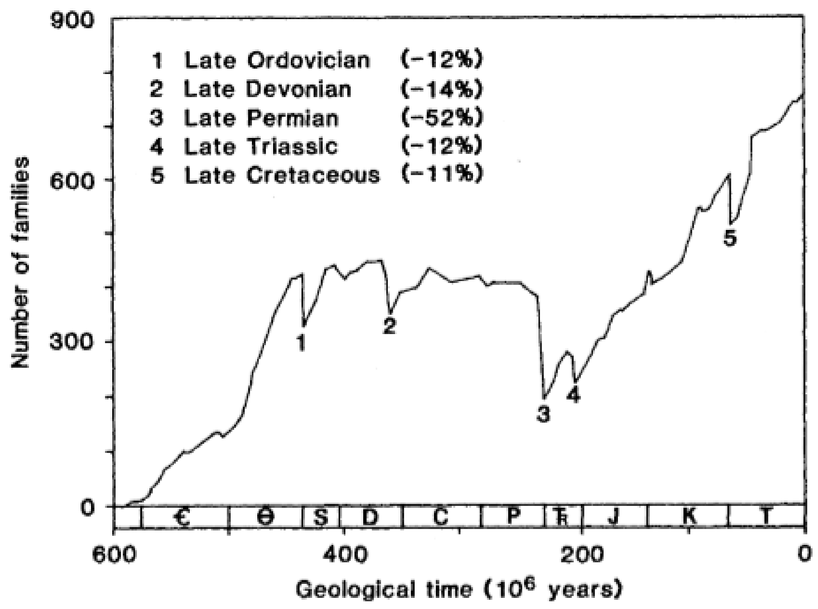

Figure 1: Five Major Mass Extinction throughout the Earth Evolutionary History. (Figure source: Seposki, 1986)

Possible causes for Late Permian Mass extinction:

- Bolide Impact (Trigger)
- Volcanism (Trigger)
- Catastrophic methane release (Trigger/Mechanism)
- *Anoxia (low oxygen) (Mechanism)*

Triggers cause the mechanism to happen. Mechanisms do the killing.

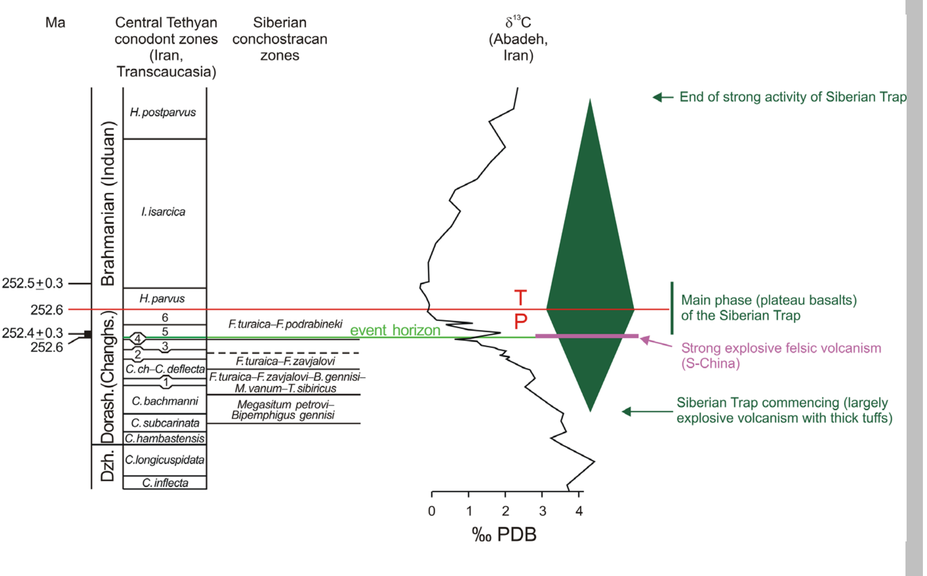

Figure 2: Global carbon isotopic excursion showing duration and intensity of mafic Siberian Trap and its impact on late Permian mass extinction event (Figure Source: Korte et al., 2010).

Objectives

- To trace sediment provenance changes across the P-T transition, if any, by investigating Sr-Nd isotopic compositions in silicate fraction of sedimentary rocks from the Guryul ravine Section, Kashmir, India.
- reconstruction of the oceanic condition of the neo Tethys at the time of this extinction event.
- To investigate the probable causes of this extinction across this Late Permian – Early Triassic Boundary at the Neo Tethys.

REFERENCES
Korte et al., 2010; Tewari et al., 2015; Mandal et al., 2021, Seposki,1986

Geological Setting and Methodology

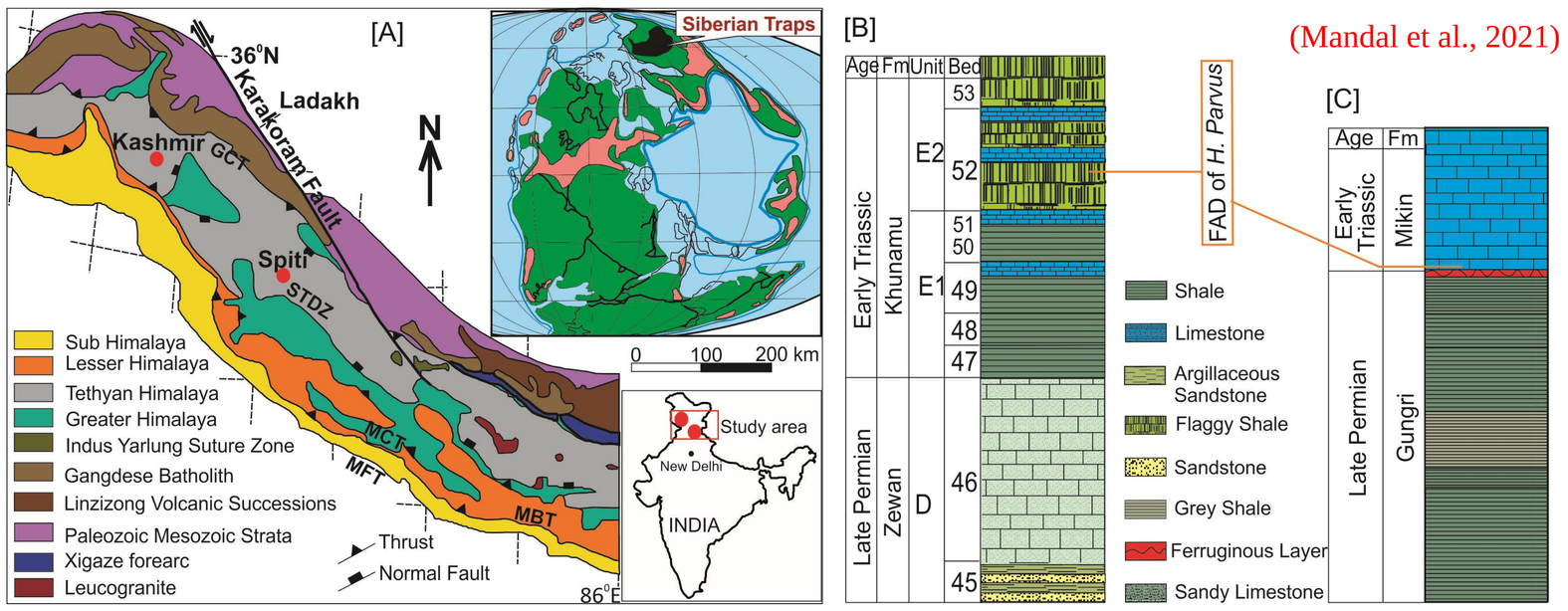

Figure 3: Geological map and Litholog across P-Tr of Guryul Ravine and Spti valley Section and the Paleogeographic map of India during Late Permian

The oceanic conditions of the Neo-Tethys during this event are well-preserved in the Guryul Ravine section (Kashmir) from the Himalaya.
These sediments were deposited in depositional settings varying from shallow to deeper shelf regions, and have not gone through any major post-depositional alteration.
Earlier studies have constrained the Permian-Triassic (P-T) boundary of the section through FAD of the *Hindeodus Parvus* in the E2 unit (bed 52) of the Khunamuh Formation.

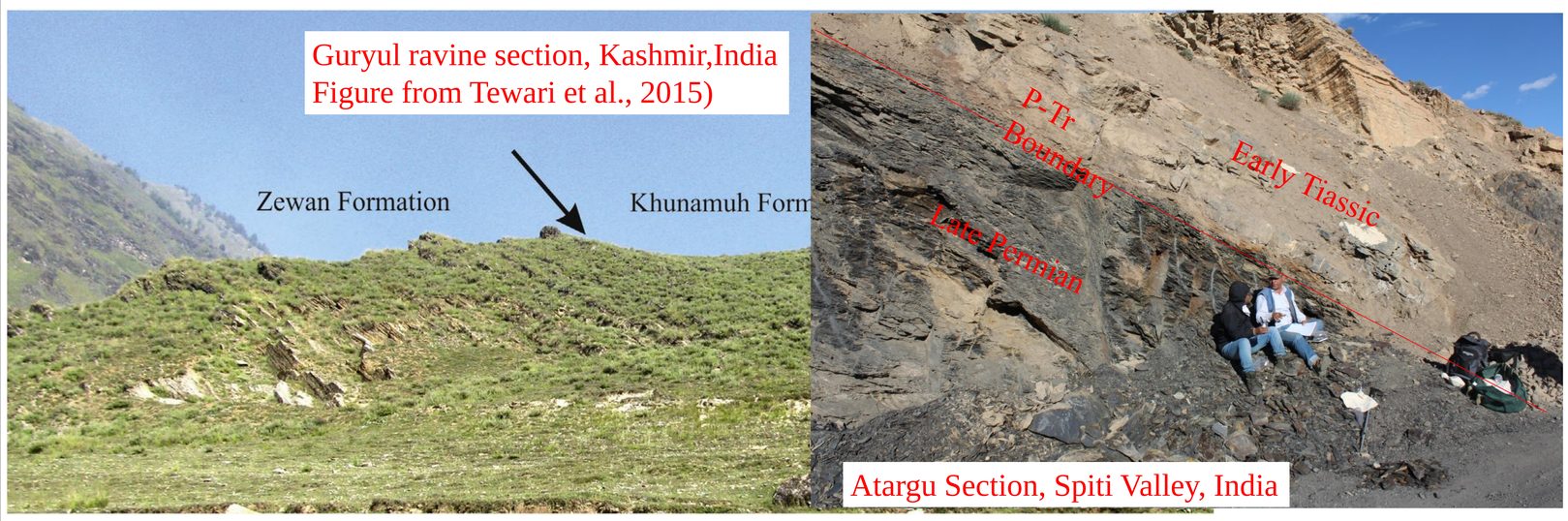

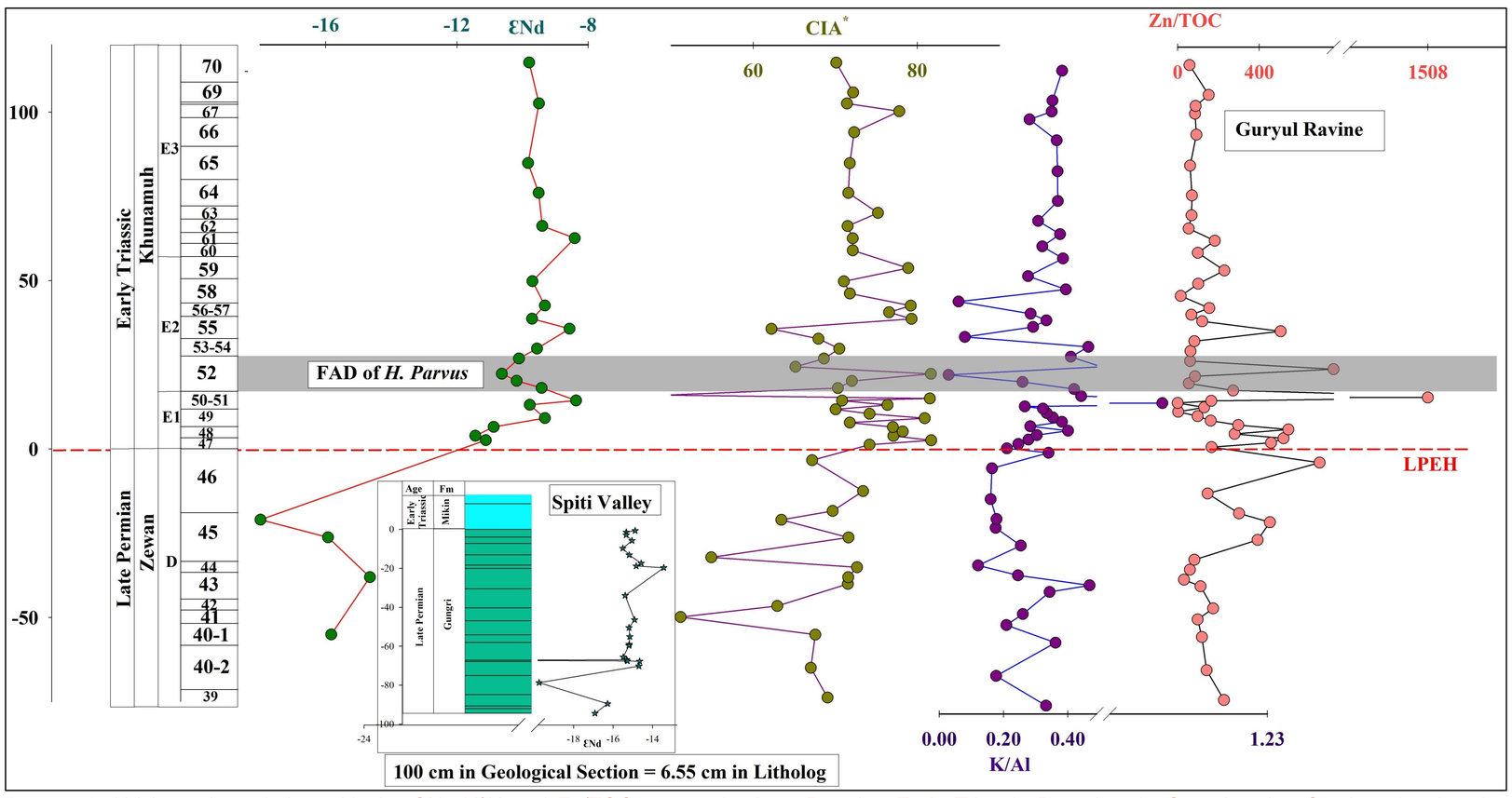

Figure 4: Nd Isotopic variation with the CIA, K/Al and Zn/TOC across the Late Permian Early Triassic Boundary in Guryul ravine Section showing the Provenances across the bounday. Inset is the Nd Isotopic changes across the Late Permian in Spiti valley secton.

The average Nd isotopic (ε_{Nd}) compositions of the Guryul samples is found lower for the Late Permian (-13 ± 3; n = 10) than the Early Triassic (-9.6 ± 0.6; n = 15) deposits.

Summary

The Nd isotopic shift around the P-T boundary points to drastic change in sediment provenances to the Neo-Tethys. higher ε_{Nd} values for the Early Triassic samples indicate a relative increase in sediment supply from the basaltic (than granitic) sources during this period. Preliminary mass balance calculations involving Nd isotopes (assuming similar Nd concentrations for provenances and samples) indicate that the sediment flux increased by about two times during this period. This increased sediment supply from basaltic sources is synchronous to the extinction horizon identified earlier for this section. These observations from our study underscore importance of volcanic sources in driving the late Permian mass extinction event.

Poster Presentation at FGRC, PRL, Ahmedabad; September 27-28, 2021

Extremely high-grade, lava-like rhyolitic ignimbrites at Osham Hill, Saurashtra, northwestern Deccan Traps: Stratigraphy, structures, textures, and physical volcanology

Anmol Naik[1] *(Email: anmolnaik@iitb.ac.in)*, Hetu Sheth[1], Janisar M Sheikh[2], Alok Kumar[2]

[1] *Department of Earth Sciences, Indian Institute of Technology Bombay, Powai, Mumbai 400076, India*
[2] *Centre of Advanced Study in Geology, Institute of Science, Banaras Hindu University (BHU), Varanasi 221005, India*

1. Introduction

In many continental flood basalt (CFB) provinces of the world, widespread silicic lavas and ignimbrites overlie the mafic lavas. The petrogenesis of these silicic magmas involves diverse mechanisms and is therefore a topic of considerable interest. Whether the extensive silicic units were erupted effusively (forming lava flows and domes), or explosively (forming pyroclastic deposits such as ignimbrites) is also an important question, especially from the point of view of the environmental impact of the volcanism. This is because explosive eruptions can inject ash and magmatic gases to much greater heights in the atmosphere than effusive eruptions, with correspondingly significantly wider distribution.

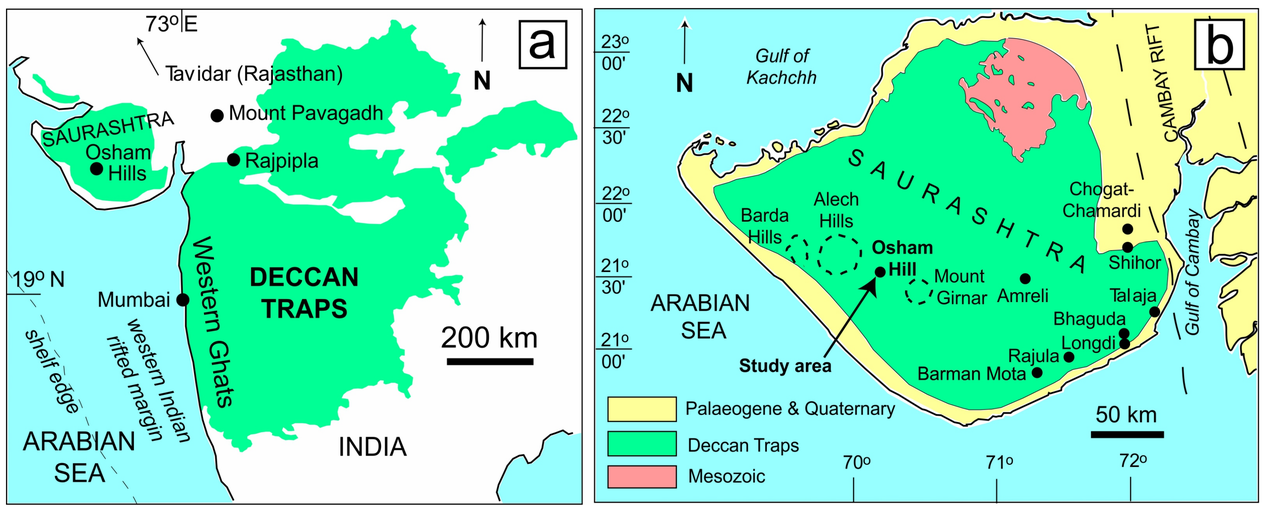

(a) Geological map of the Deccan Traps CFB province (light green) showing the location of Osham Hill, the study area. (b) Geological map of the Saurashtra peninsulas. Filled circles (in a and b) denote other localities with notable rhyolites and dacites.

2. Regional geology

Our knowledge of this post-flood basalt silicic volcanism in the Deccan Traps CFB province of India remains limited. In the 65.5 Ma Deccan Traps CFB province of India, covering 500,000 km^2 in west-central India, silicic rocks (rhyolites, dacites, and granophyres) are volumetrically minor (~1% of preserved volume). However, they are abundant in the northwestern and northern parts of this province, particularly the Saurashtra peninsula. Here we describe the stratigraphy, structures, and textures of the rhyolites of Osham Hill in Saurashtra, in the northwestern Deccan Traps.

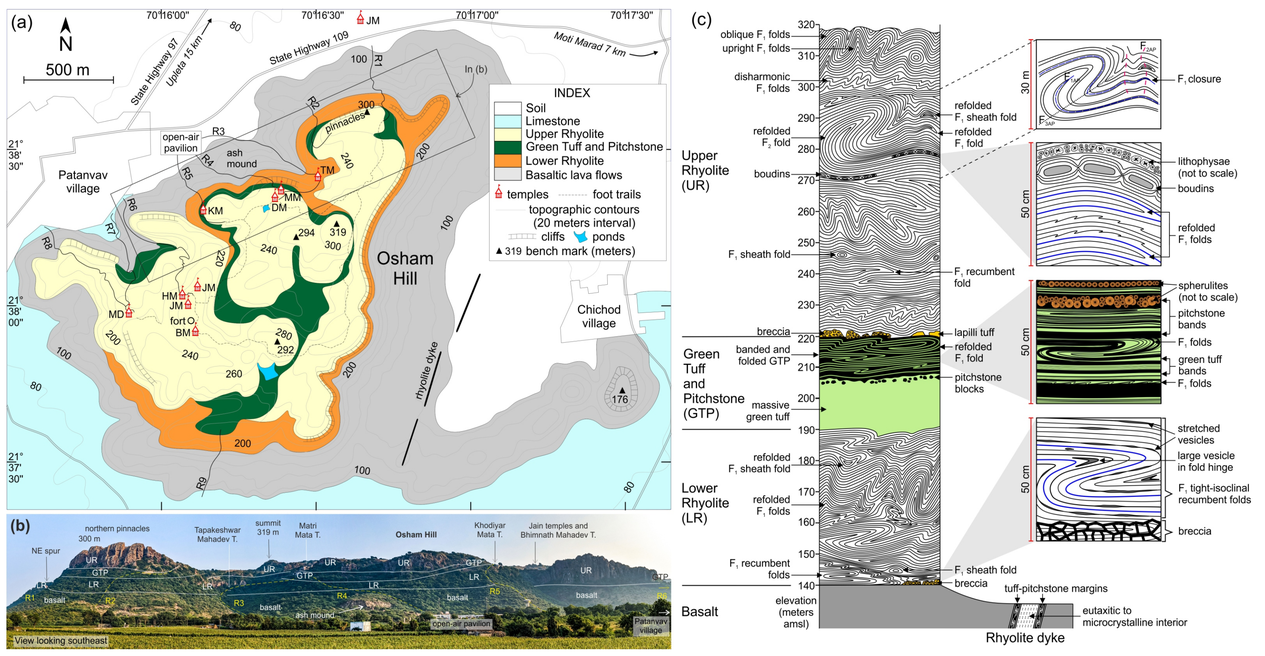

(a) Geological map of Osham Hill. (b) Panoramic views of Osham Hill showing the topographic features, the major eruptive units (c) Graphic log of a typical section through the Osham rhyolites, showing their eruptive stratigraphy and typical outcrop structures and other features.

3. Stratigraphy, structures and textures

Basaltic lavas forming the lower parts of the hill are overlain by the "Lower Rhyolite" (LR), which is tens of meters thick and shows intense rheomorphic deformation (flow banding and folding) at microscopic, outcrop, and tens of meters scales. The LR is overlain by a "Green Tuff and Pitchstone" (GTP) band 20-40 m thick, containing massive green tuff to strongly rheomorphic, commonly spherulitic pitchstone, both types showing sharp but irregular contacts. The GTP is overlain by the "Upper Rhyolite" (UR), with an ~100 m preserved thickness. This resembles the LR in many structural features, and also contains a thin (~1 m), laterally discontinuous basal layer of unbedded, nonwelded lapilli tuff. The LR and UR locally contain basal autobreccias which are unlike crumble breccias of rhyolitic lava flows. In thin section the LR and UR are microcrystalline and lava-like, though they contain many relict vitroclasts (glass shards and pumice fragments). The LR also shows rare millimeter-size basaltic lithic clasts. The GTP contains abundant vitroclasts.

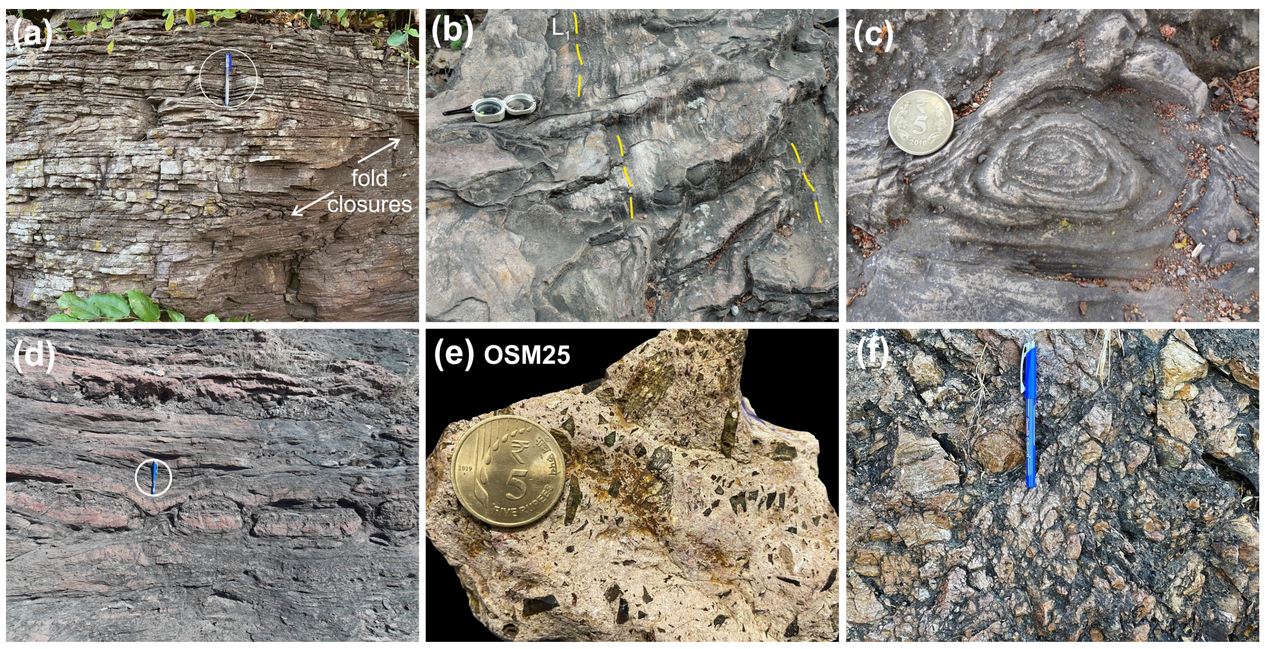

Outcrop structures of the Lower Rhyolite (LR) and Upper Rhyolite (UR). (a) *Recumbent isoclinal folds.* ***(b)*** *Curvilinear fold hinges and elongation lineation L_1 which varies from transverse to subparallel to fold axes.* ***(c)*** *Small F_3 sheath fold.* ***(d)*** *Well-developed boudins of a large flow band.* ***(e)*** *Hand specimen of the massive, nonwelded tuff.* ***(f)*** *Autobreccia of intensely flow-banded and flow-folded LR.*

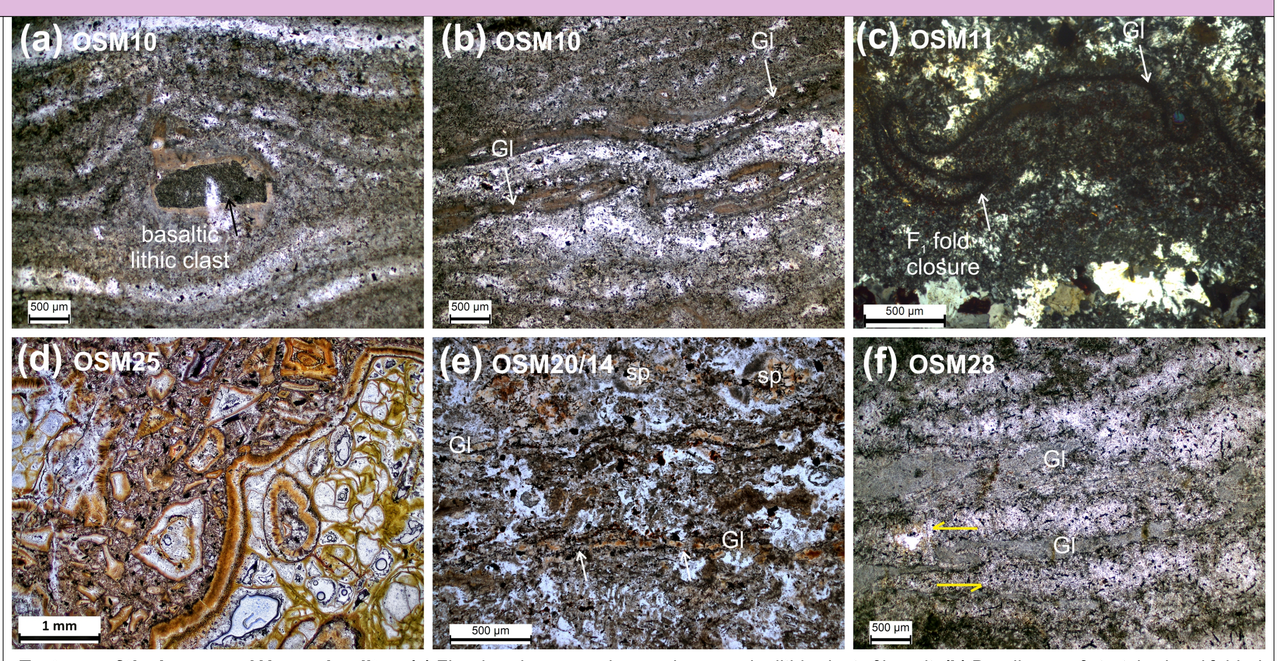

Textures of the Lower and Upper rhyolites. (a) *Flow bands wrapped around an angular lithic clast of basalt.* ***(b)*** *Boudinage of stretched and folded glass shards.* ***(c)*** *An F_1 fold closure and F_2 folds in a glass shard (LR).* ***(d)*** *Lapilli tuff showing an abundance of cuspate glass shards* ***(e)*** *Folded and boudinaged glass (UR).* ***(f)*** *Well-preserved, stretched and asymmetrically folded glass shards*

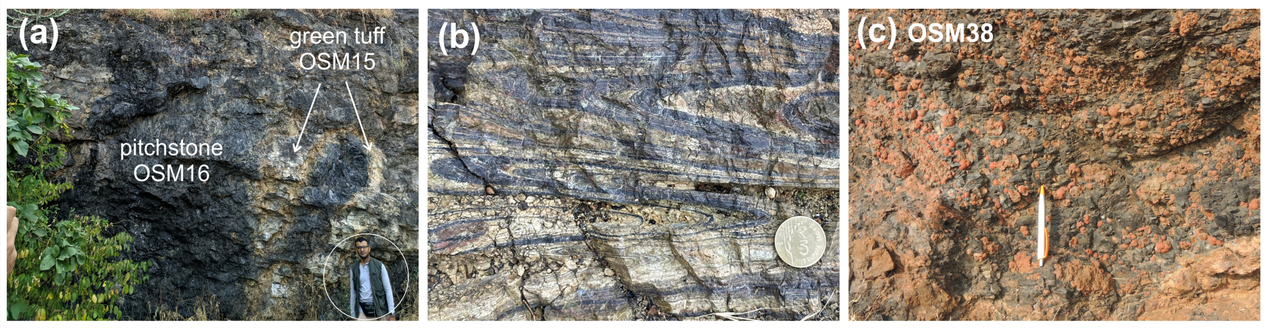

Outcrop structures and textures of the GTP (a) *Sharp and irregular contacts between green tuff and flow-banded pitchstone.* ***(b)*** *Isoclinal folds in tuff-pitchstone bands.* ***(c)*** *Pervasively spherulitic southern pitchstone band.* ***(d)*** *Closely packed glass shards in green tuff.* ***(e)*** *Flow banding (S_{0-1}) in pitchstone.* ***(f)*** *A cluster of microscopic-sized spherulites growing on each other and across existing flow bands in pitchstone.*

4. Physical Volcanology

- We interpret the LR and UR as extremely high-grade, intensely welded, lava-like ignimbrites, and the GTP as a low-grade ignimbrite with varying degrees of welding and rheomorphic deformation. The interpretation of the LR and the UR as extremely high-grade, lava-like ignimbrites, and that of the GTP unit as a lower-grade ignimbrite, implies deposition from a series of pyroclastic density currents in rapid succession.
- The absence of sedimentary interbeds and soil horizons suggests that the whole Osham ignimbrite sequence was deposited subaerially and rapidly, without eruptive breaks.
- The lava-like characteristics of the LR and the UR may reflect formation of the pyroclastic density currents from relatively low eruption columns and a "boil over" eruption style, with minimal pyroclast cooling during transport, and this may be due to very high eruption rates, a wide conduit, or both . In contrast, the pumice and

5. Eruptive Vents

The eruptive vent locations are unknown. However, a rhyolite dyke intruding basalts at the southeastern end of Osham Hill is pyroclastic, showing a eutaxitic to microcrystalline interior and margins of welded and rheomorphic tuff-pitchstone. Basaltic lithic fragments found in the dyke margins suggest that it may be the

Outcrop structures and textures of the rhyolite dyke (a) *The gentle (5°) westerly dip of the basalts and the sharp topographic ridge formed by the dyke.* ***(b)*** *Dyke margins of welded tuff-pitchstone.* ***(c)*** *Vertical flow banding wrapped around a basaltic lithic clast.* ***(d)*** *Plan view of asymmetric folds with a sinistral shear sense exposed in a horizontal face of the welded tuff-pitchstone.* ***(e)*** *Abundant small pumice fiamme (white) in the eutaxitic central part of the dyke.* ***(f)*** *Intense and asymmetric folding of flow bands.* ***(g)*** *Rotated basaltic lithic clast with surrounding microfolds.*

Naik acknowledges CSIR for PhD senior research fellowship; File no.: 09/087(0908)/2017-EMR-I

Presented by Anmol Naik at the Frontiers in Geosciences Research Conference, PRL, September 2021

SIGNIFICANCE AND ROLE OF CONTROLLING FACTORS IN THE CHEMICAL WEATHERING OF AMPHIBOLITE: AN OVERVIEW

Khalid Mohammed Ghasera and Shaik. A. Rashid
Dept. of Geology, Aligarh Muslim University, Aligarh

Introduction

Chemical weathering of continental rocks leads to irreversible decomposition of thermodynamically unstable rock constitutes at the Earth's surface. The interaction between these rocks and interrelated weathering agents (e.g., temperature, precipitation, relief, vegetation, etc.), commences with changes in environmental conditions, in order to achieve stability under certain natural conditions.

The process of weathering itself is controlled by several variable factors such as lithology, topography, climate, vegetation and time. However, the regional and micro variations of these factors control the progressive changes in the intensity of weathering and advancement of weathering front.

Few studies investigated rate of chemical weathering with respect to the altitudinal variations; however, these variations were on small scale. Which concluded that temperature is the main controlling factor of chemical weathering process.

The aim of this review is to evaluate the chemical characteristics of in-situ weathering profile developed on amphibolite rock at different geographical altitudes and climatic zones and infer variations in controlling factors.

Data Collection

The data were collected from indexed publication in the English language on amphibolite weathering. Despite the few numbers of publications on amphibolite weathering profile, we have considered the variability of controlling factors of chemical weathering. The chosen weathering profiles were from three different climatic zones viz. tropical, semi-arid and humid subtropical zone. Moreover, these profiles vary in altitude (245 m, 600 m, 908 m, 2000 m, and 2400 m).

Data analysis

In order to envisage weathering process from each location, the weathering indices and ternary plot to evaluate weathering progress. These indices as in the table:

Index	Formula	Reference
Chemical Index of Alternation (CIA)	CIA=100 [Al_2O_3/(Al_2O_3 + CaO + Na_2O + K_2O)]	Nesbitt and Young (1982)
Chemical Index of Weathering (CIW)	CIW = 100 [Al_2O_3/(Al_2O_3 + CaO + Na_2O)]	Harnois (1988)
Plagioclase Index of Alteration (PIA)	PIA = 100 [(Al_2O_3–K_2O)/(Al_2O_3 + CaO + Na_2O – K_2O)]	Fedo et al. (1995)
Mafic Index of Alteration (MIA)	MIA = 100 [(Al_2O_3+ Fe_2O_3 /(Al_2O_3 + Fe_2O_3+ MgO + CaO + Na_2O + K_2O)]	Babechuk et al. (2014)
Ternary diagram		
A-CN-K	Al_2O_3 - CaO + Na_2O - K_2O	Nesbitt and Young (1984)
A-CNK-FM	Al_2O_3 - CaO + Na_2O + K_2O - Fe_2O_3+ MgO	
Relative mobility (RM)	RM = [(Cs / Cp)-1] × 100	Sharma and Rajamani (2000)

Where Cs is concentration of the element in weathered sample, and Cp concentration of the element in parent rock.

Weathering intensity and Weathering trend

There are two main factors distinguishing the weathering development in these profiles:

a-***Precipitation.***

b-***Altitude***.

- *Low precipitation*: at 600 m and 908 m.
  - Less or incipient weathering process.
- *High precipitation*: at 245 m, 2000 m, 2400m.
  - Advanced weathering development at 245 m and 2000 m.
  - Intermediate weathering process at 2400 m

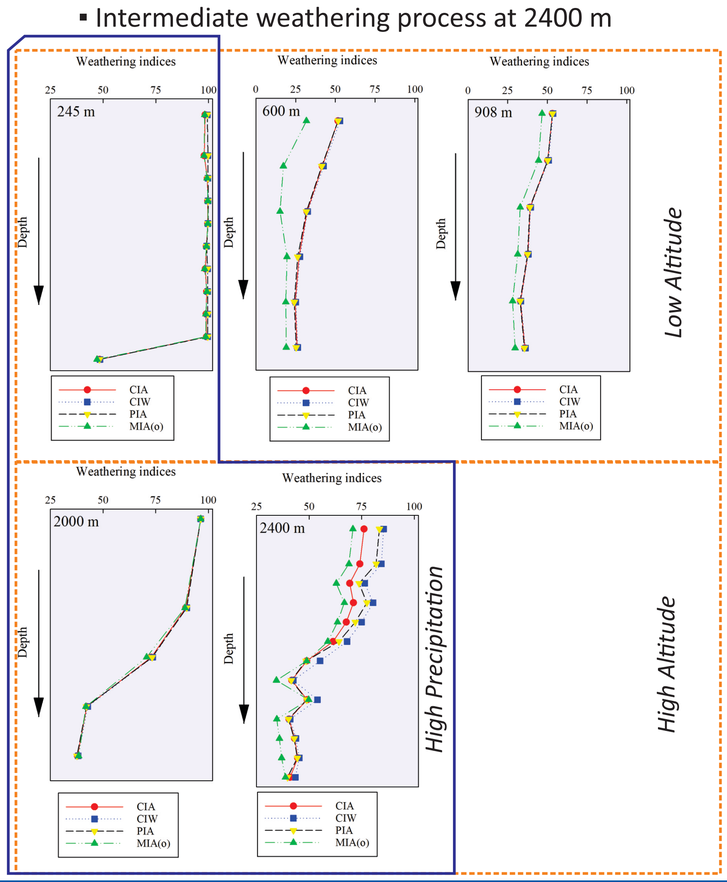

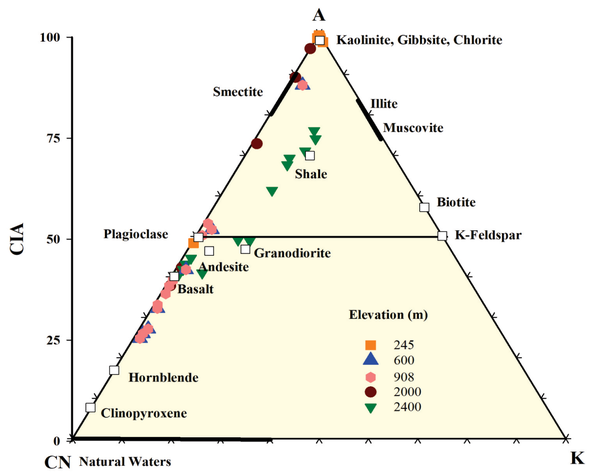

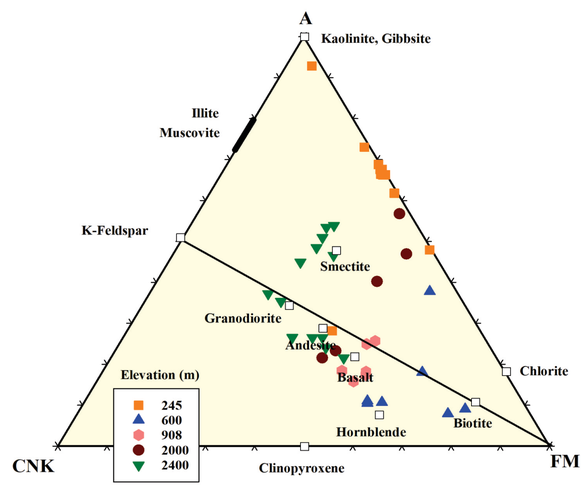

In A-CN-K diagram, the samples are plotted sub-parallel to A-CN line with general trend portrays the continuous leaching of Ca and Na from profile and enrichment of Al, ensuing plagioclase decomposition. In 2400 m profile, there is a little shift in this trend on K-feldspar join from that of normal basalt trend, which may be due to increases in K content with advanced weathering conditions. It is known that biotite and hornblende are K-bearing constituents in amphibolite rock. Transformation of biotite into clay mineral is responsible of K content in early weathering stage whereas hornblende resists weathering in this stage. A-CNK-FM diagram reveal removal of Fe and Mg from the profile with weathering advancement.

Elements Mobilization

The Elements mobility shows various trends in each profile. Alkali oxides removed from all profile, with exception for K_2O. Al_2O_3 display enrichment as the weathering commences. Other oxides show variations in their mobility, which indicate variety in controlling factors (pH, Eh, vegetation organic matter…etc.), which determine the fate of certain element.

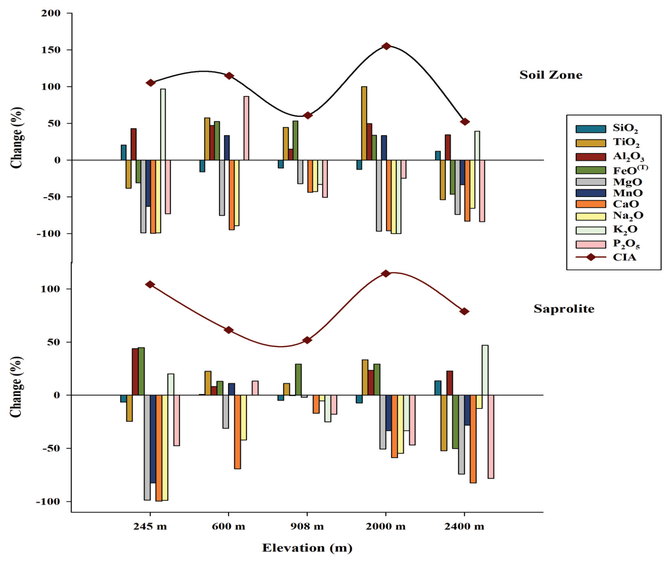

Regional Controlling Factors

Away from the local factors which may affect weathering process and elemental mobility, the regional factors in terms of climate zone, geographical elevation and tectonic stability of the region are the main controlling factors. .

In these locations, amphibolite profiles, precipitation is the main drive factor of weathering process, thus profiles at 245 m, 2000 m, 2400 m, showed advanced weathering intensity, in comparison to 600 m, 908 m, where precipitation is less.

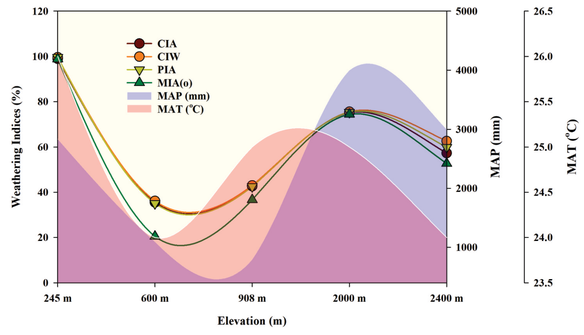

Temperature range also show variation at these locations and that may explain the variation in weathering extent. Hence, weathering progress is deep at 245 m due to short range of temperature compare to other locations.

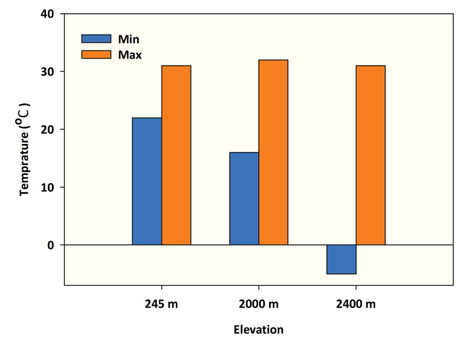

Another factor, which could affect weathering process is tectonic stability of the region. In case of profiles at 2000 m and 2400 m, both receiving almost same amount of rainfall, but the tectonic activity and high earthquake frequency might disturb weathering advancement by enhancing drainability of rock; hence, the fine particles and solution find pathway from profile.

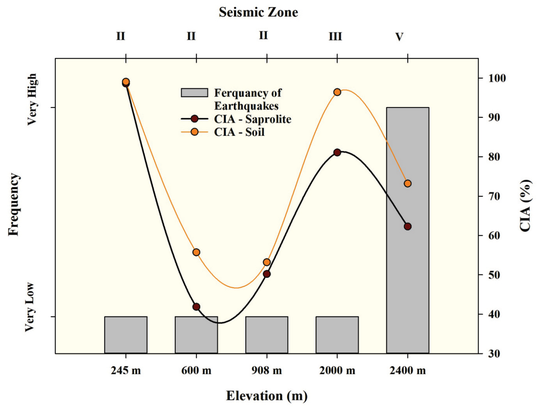

Conclusion

- Controlling factors of elemental mobility are location-specific factors, and differ from element to another.
- Geographical altitude has indirect effect on weathering process via controlling regional climate.
- Precipitation is the most important factor in chemical weathering.
- Temperature range has a significance role in weathering process.
- Tectonic stability of the region influences the maturity of in-situ weathered products.

References

Babechuk M, Widdowson M and Kamber B (2014) Quantifying chemical weathering intensity and trace element release from two contrasting basalt profiles, Deccan Traps, India; Chemical Geology 363 56-75.

Fedo CM, Nesbitt HW and Young GM (1995) Unraveling the effects of potassium metasomatism in sedimentary rocks and paleosols, with implications for paleoweathering conditions and provenance; Geology, 23 921-924.

Harnois L (1988) The CIW index: a new chemical index of weathering; Sedimentary Geology 55 319-322.

Nesbitt HW and Young GM (1982) Early Proterozoic climates and plate motions inferred from major element chemistry of lutites; Nature 299 715-717.

Nesbitt HW and Young GM (1984) Prediction of some weathering trends of -plutonic and volcanic rocks based on thermodynamic and kinetic considerations; Geochimica et Cosmochimica Acta 48 1523-1534.

Sharma A and Rajamani V (2000) Major element, REE, and other trace element behavior in amphibolite weathering under semiarid conditions in southern India; The Journal of Geology 108 487-496.

Aligarh Muslim University

Department of Geology
AMU Campus, Aligarh, Uttar Pradesh 202002
www.amu.ac.in

Evolution of Kamthai carbonatites: Evidence from Geochemistry

Milan K. Mahala[1] and Jyotiranjan S. Ray[1,2]

[1]Geosciences Division, Physical Research Laboratory, Ahmedabad-380009, India

[2]Solid earth research group, National center for earth science studies, Akkulam, Thiruvananthapuram, 695 011, India

Introduction

Carbonatites are unique carbonate bearing mantle derived rocks. Carbonatite magmas have very low density and viscosity, and are extremely rich in incompatible trace elements. Because of these properties, they get emplaced rapidly without significant crustal contamination, and therefore, they are regarded as one of the best record keepers of the mantle evolution. In spite of more than forty years of research, some of the questions on the origin of these rocks remain unanswered; such as (1) the nature of the genetic link between the carbonatites and associated alkaline silicate rocks, (2) the source of carbonate melts in the mantle (lithosphere vs. asthenosphere) and (3) source of carbon in carbonatites (primordial vs. recycled). In this regard, Kamthai carbonatite-alkaline complex, being located in Rajasthan, India and a suspected member of Deccan alkaline province (Basu *et al.*, 1993; Chandra *et al.*, 2019) provides an excellent opportunity to understand their temporal and genetic linkage with the plumes. Recently, evidences of older alkaline magmatism separated by 20 Ma has been reported suggesting the role of lithosphere behind the multiple magmatism (Sheth *et al.*, 2017). Being the host of both the carbonatites and alkaline silicate rocks, an investigation about the genetic linkage of the carbonatites with the associated alkaline silicate rocks is of paramount importance.

Study Area, Materials and Methods

- Kamthai carbonatite-alkaline complex is located on the eastern side of the Barmer rift, Rajasthan, India.
- Trace element measurements of representative whole rock carbonatites and alkaline rocks were measured in a Thermo Q-ICPMS.
- Fresh carbonate powders were micro drilled from carbonatites and alkaline rocks to measure C and O isotopic ratios in a Thermo IRMS (MAT-253).
- After acid digestion of the whole rock carbonatite and alkaline rock powders,Sr was separated by cation exchange chromatography using Biorad AG50W-X8 (200-400 mesh) resin and Nd was separated using Ln-specific resin from Eichrom. $^{87}Sr/^{86}Sr$ and $^{143}Nd/^{144}Nd$ were measured in a Thermo Triton plus TIMS.
- Ar-Ar dating of one Phlogopite mineral separate from a carbonatite dike and 4 phonolite dikes from carbonatite was done at IIT, Bombay.

A

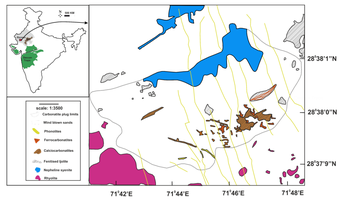

B

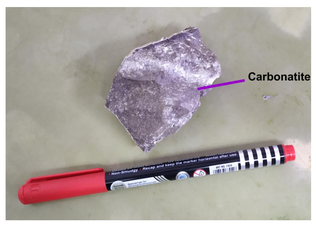

C

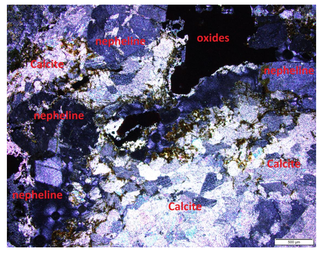

- Figure A: Geological map of Kamthai carbonatite-alkaline complex, Rajasthan, India (modified after Bhushan, 2015)
- Figure B: A representative carbonatite sample from Kamthai, Rajasthan
- Figure C: Crossed polar view of a carbonatite containing calcites, nephelines as phenocrysts.

- The long term reproducibility of TIMS Triton plus (PRL) for Sr, Nd is measured to be 30 ppm and 20 ppm respectively.
- The accuracy of BHVO-2, AGV-2 standards measured in Q-ICPMS is better than 8% for all trace elements.
- The precision of IRMS (MAT-253) for both the $\delta^{13}C$ and $\delta^{18}O$ values was less than 0.01 ‰.

Results and Discussion

- Ar - Ar age of all the samples determined are of same age (~68.5 (±2) Ma). This supports the theory of an early pulse of Deccan-Reunion plume magmatism (~65.5 Ma) . (Fig A)
- $\delta^{13}C$ and $\delta^{18}O$ values of unaltered carbonatites fall in the mantle field, which suggest that the carbonatites are derived from the mantle. . (Fig B)

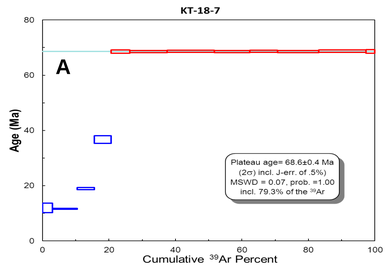

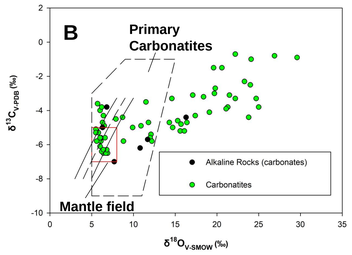

- The carbonatites are enriched in light rare earth elements as compared to heavy rare earth elements in a chondrite normalized plot. The enrichment of REEs in many altered carbonatites reaches upto wt% level making them as highly potential candidates for REE exploration. . (Fig C)
- Carbonatites and alkaline rocks have similar incompatible ratios (e.g., Ba/Nb, Nb/La) as that of Reunion island basalts indicating their genetic linkage to Reunion plume. . (Fig D)

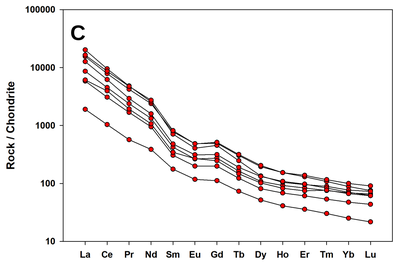

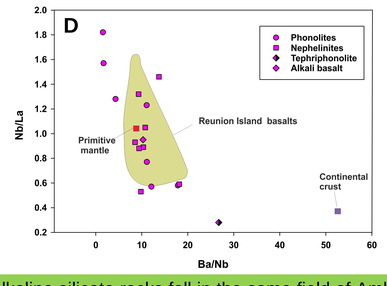

- Initial $^{87}Sr/^{86}Sr$ and εNd of carbonatites and alkaline silicate rocks fall in the same field of Ambenali basalts of Deccan flood basalt province which is believed to have been originated from the plume. Their close proximity to present day Reunion basalts again supports their derivation from a plume source. (Fig E)

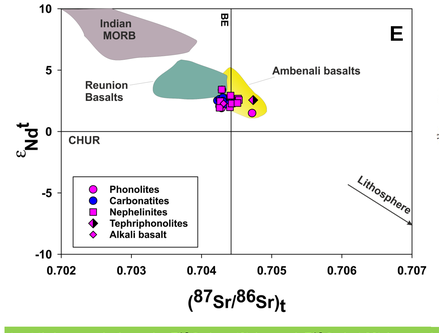

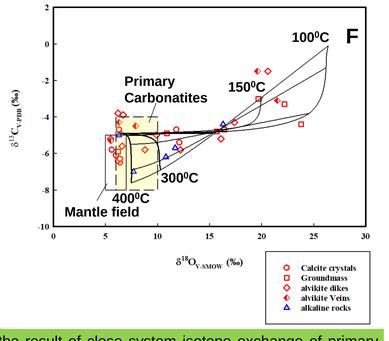

- Higher variations in $\delta^{13}C$ (> -4‰) and $\delta^{18}O$ (>12‰) are the result of close system isotope exchange of primary carbonatites with a H_2O–CO_2 bearing magmatic fluid with $\delta^{13}C$ value of -4‰ and $\delta^{18}O$ value of 5.5 ‰ and molar oxygen ratio of 0.1 at different temperatures (400^0C-100^0C) . (Fig F)

Summary

- The origin of Kamthai carbonatite-alkaline complex, a suspected member of end cretaceous Deccan alkaline province which is beleived to have originated from Deccan-Reunion plume magmatism between 65-69 Ma, is putative because of the recent findings of older magmatic (~88 Ma) event unrelated to Deccan magmatism in the complex. The complex also hosts carbonatites and alkaline rocks in same outcrop, whose genetic relationship is not well constrained.
- 68.5 (± 2) Ma Ar-Ar age for the carbonatites and alkaline rocks suggest that carbonatite-alkaline magmatism was coeval and they supports their genetic linkage to Reunion plume.
- Stable C and O isotopic composition reveals that carbonates from both carbonatites and alkaline rocks have the signature of primary igneous rocks ($\delta^{13}C$< -4‰, $\delta^{18}O$<12‰) derived from mantle. however some of the carbonatites that display higher variations in $\delta^{13}C$ and $\delta^{18}O$ values are the result of post magmatic alteration by secondary magmatic fluid having $\delta^{13}C$ = -4‰ and $\delta^{18}O$= 5.5‰ between 400^0C to 100^0C. Variations among primary carbonatites can be ascribed to fractional crystallization of calcites from a carbonatite magma (Ray J.R. and Ramesh R., 2000).
- Trace element studies reveal that carbonatites have chondrite normalised enriched incompatible element trend compared to heavy rare earth elements, which suggests they are derived from an enriched mantle source. Associated alkaline silicate rocks have similar incompatible element ratios as that of reunion plume basalts.
- Sr, Nd isotopic studies reveal that carbonatites and alkaline rocks had similar initial $^{87}Sr/^{86}Sr$ and εNd, which suggests they were derived from a similar source corroborating the genetic relationship theory between the two rock types. Their initial $^{87}Sr/^{86}Sr$ and εNd also are close to Ambenali basalts of Deccan flood basalt province which is believed to have a plume component. Initial $^{87}Sr/^{86}Sr$ of Carbonatites and alkaline rocks are close to bulk earth values supporting their derivation from a deeper mantle (plume source).
- Present day Reunion basalts are relatively more depleted (higher εNd values), and if recent volcanism in Reunion islands incorporates the shallow (depleted) mantle, then Kamthai carbonatites and alkaline rocks having a lesser εNd may represent the earliest enriched components of Reunion plume.

Conclusions

Some of the key findings of this study are

- **Kamthai carbonatite-alkaline complex had been emplaced 68.5 Ma ago, which supports their temporal linkage to Deccan flood basalt vocanism.**
- **Carbonatite and alkaline magmatism had taken place during the same period time supporting the theory that they may have been derived from the same parental magma.**
- **Carbonatites have inherited their magmatic signature and are derived from the mantle. Carbonatites and alkaline rocks are derived from an enriched mantle source.**
- **Carbonatites and alkaline rocks support their origin in a plume setting.**

Acknowledgments

We thank Dr. Anil D. Shukla for his help during the trace element analysis. The author is also greatly thankful to Dr. Dwijesh Ray for his help during XRD analysis. The author is thankful to Dr. Arvind Singh for his contribution in the research work. We give special thanks to Dr. Ikshu Gautam, Dr. Bivin Geo George , Jitender Kumar for their help in the analysis.

References

- Basu, A. R. *et al.* (1993) 'Early and Late Alkali Igneous Pulses and a High 3He Plume Origin for the Deccan Flood Basalts', *Science*, 261(5123), pp. 902–906. doi: 10.1126/science.261.5123.902.
- Chandra, J. *et al.* (2019) 'The Origin of Carbonatites from Amba-Dongar within the Deccan Large Igneous Province', *Journal of Petrology*, 60(6), pp. 1119–1134. doi: 10.1093/petrology/egz026.
- Ray J.R. and Ramesh R. (2000) 'Rayleigh fractionation of stable isotopes from a multicomponent source', *Geochimica et Cosmochimica Acta*, 64(2), pp. 299–306.
- Sheth, H. *et al.* (2017) 'Recurrent Early Cretaceous, Indo-Madagascar (89–86 Ma) and Deccan (66 Ma) alkaline magmatism in the Sarnu-Dandali complex, Rajasthan: 40Ar/39Ar age evidence and geodynamic significance', *Lithos*, 284–285, pp. 512–524. doi: 10.1016/j.lithos.2017.05.005.

Lithospheric Velocity Structure Beneath the Chhotanagpur Plateau, India Using Waveform Modeling of Shear-Coupled PL Wave

Mukesh Kumar Das* and Mohit Agrawal

Indian Institute of Technology (Indian School of Mines), Dhanbad, Jharkhand

*E-mail: mukesh.17dr000318@agp.iitism.ac.in

ABSTRACT

The presented research utilizes the constraints imposed by Shear-coupled PL (SPL) wave and its associated phases to decipher seismic velocity structures of the crust and upper mantle beneath the Chhotanagpur Plateau, India. For this purpose, the best quality teleseismic earthquakes' waveform from broadband data of magnitude between 5.5 to 8.0, focal depth ≥ 300 km, and epicentral distances between 300 and 700 are extracted from seismic stations located at Dhanbad (DHN), Bokaro (BOKR), Petarwar (PTWR), Khunti (KNTI) and Sahibganj (SBG). A modified form of reflectivity method is consulted to generate synthetic seismograms for various angular frequencies where the calculation of response matrices is distributed over various nodes of the High-Performance Computing (HPC). The forward calculation is benefitted from thirty two nodes of HPC to significantly reduce the computation time. The crustal thickness of the study area varies between ~40.5 km and ~45.6 km. The thickest and thinnest crust are reported on the NE and SW parts of the study area underneath seismic stations SBG and KNTI, respectively. The observed thick crust for SBG may be due to the subsidence of the Indian lithosphere beneath the Himalayan footprint. A low-velocity zone in upper-crust observed in seismic station SBG due to the sediment deposition of Ganga-Koshi formation. The statistical tools such as the Posterior Probability Density function (PPD) and Parameter Correlation matrices (PCM) are used to find the uncertainties around best-fitting models and assess the trade-off between model parameters in the modeling scheme.

INTRODUCTION

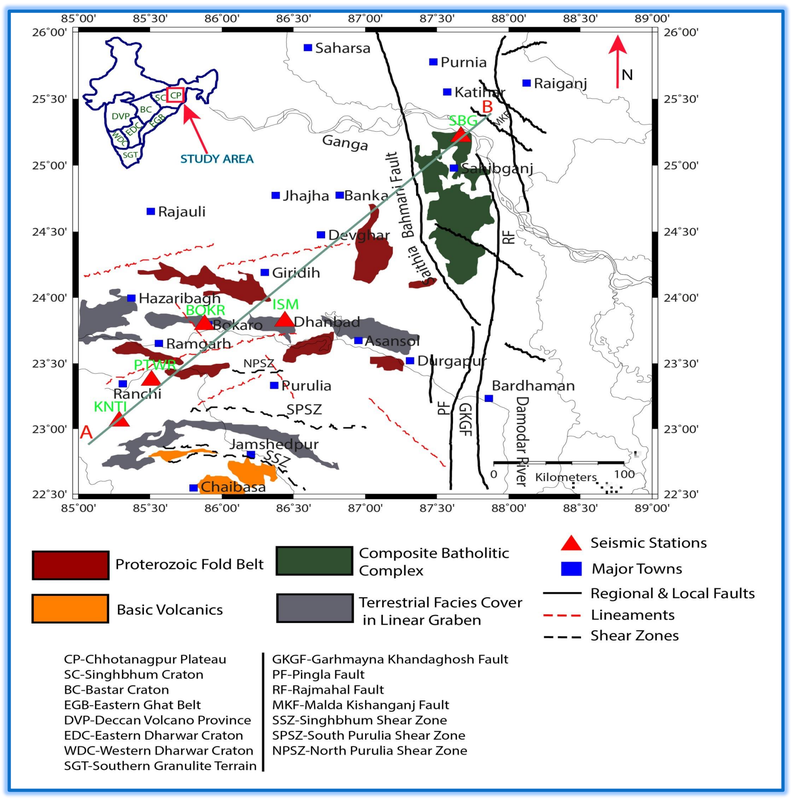

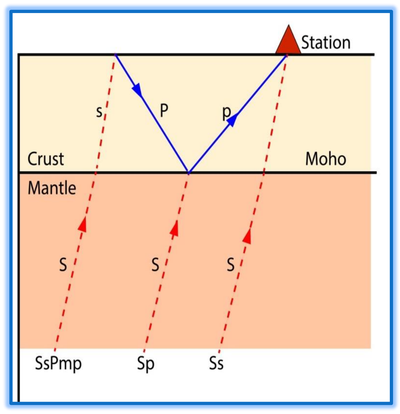

SPL generation ray path

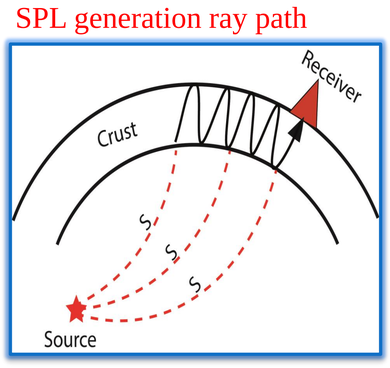

RESULTS

Obs vs Syn waveform match

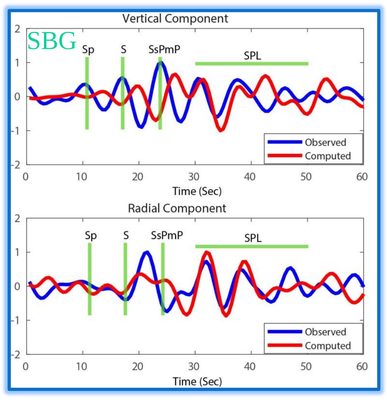

Prograde elliptical PM plot

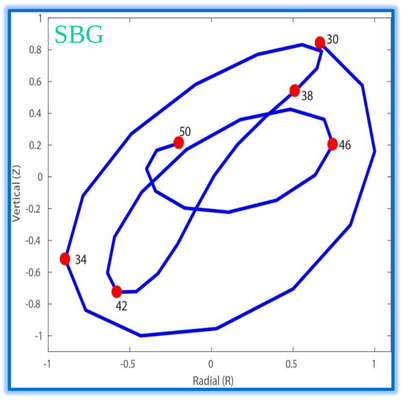

Misfit error vs iterations plot

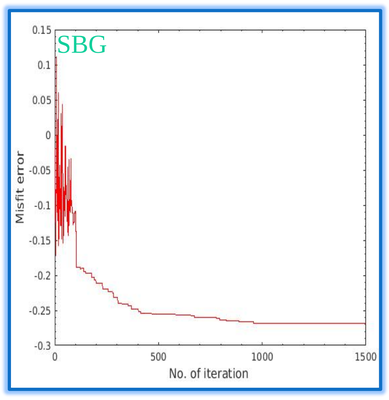

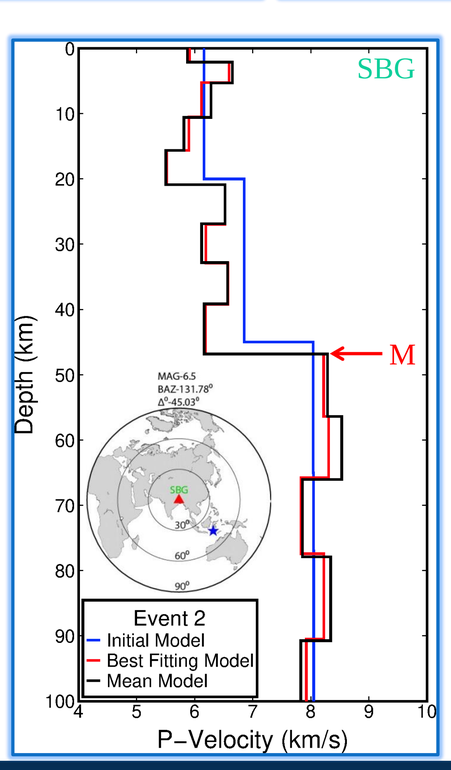

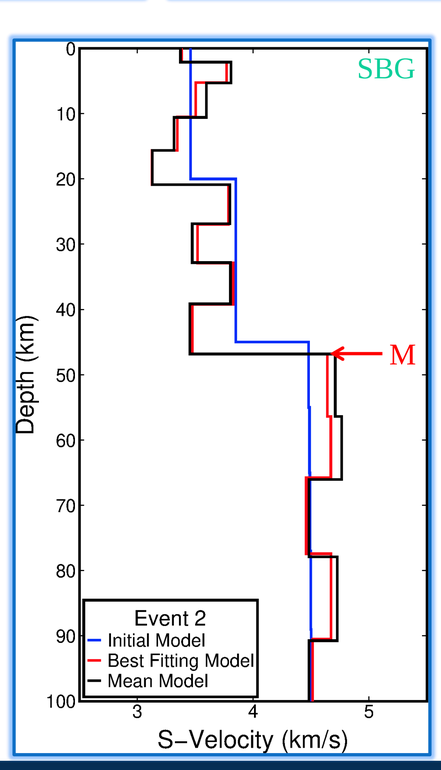

H-κ stacking for SBG

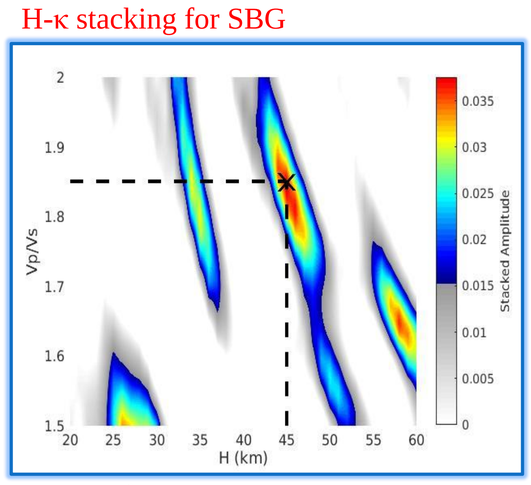

Vp PPD for SBG

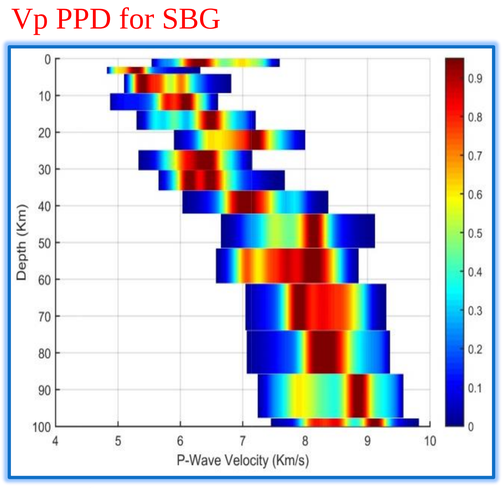

Vs PPD for SBG

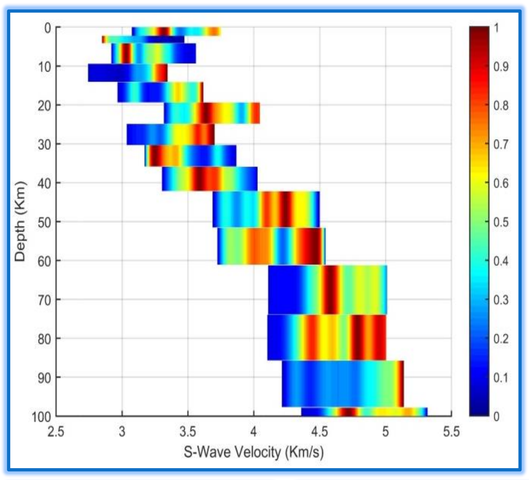

PCM for SBG

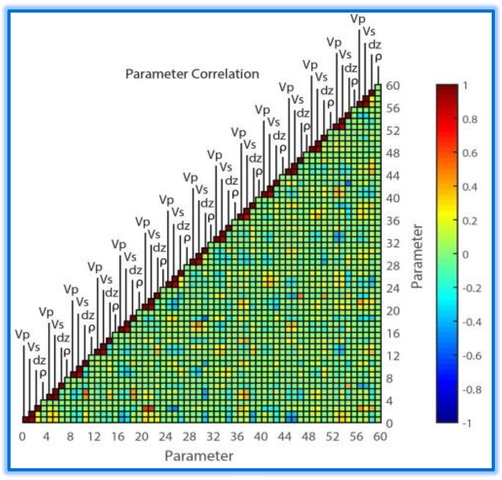

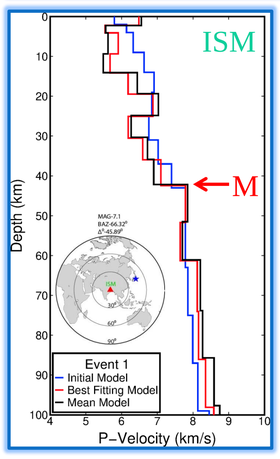

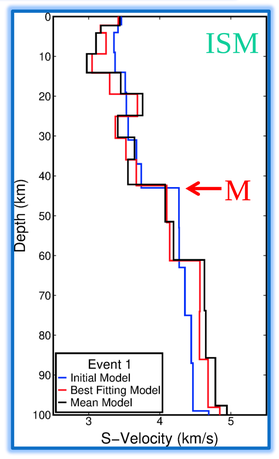

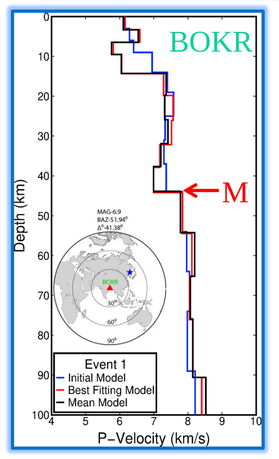

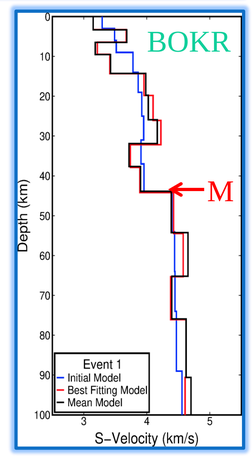

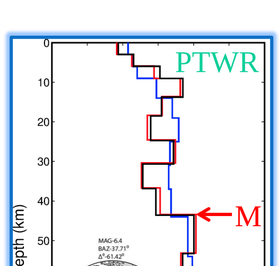

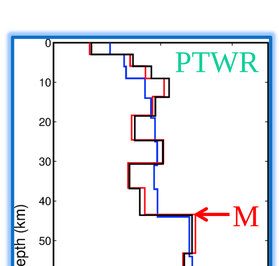

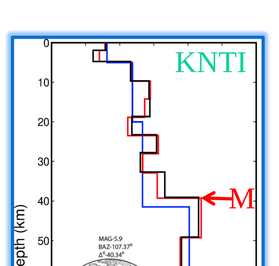

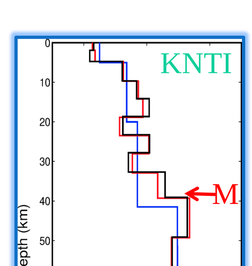

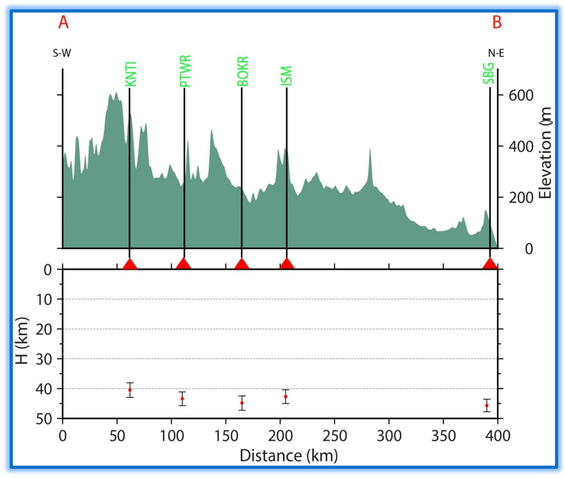

CONCLUSIONS

- **The higher average crustal Vp value 7.05 km/s and Vs value 3.80 km/s reported for seismic station BOKR, which are higher crustal values among all five stations.**
- **The thickest crust has been reported in South-West of the study area while, the thinnest crust has been reported in North-East part.**
- **A low-velocity zone in the upper crust beneath seismic station SBG reported from this study may due to the deposition of sediments from Ganga-Koshi formations.**
- **The statistical tools PPDs, and PCM provides the information about the estimated best-fitting models are well or less constrains.**

REFERENCES

- Agrawal, M., Das, M.K., Kumar, S. & Pulliam, J. (2021) Mapping lithospheric seismic structure beneath the Shillong plateau (India) and adjoining regions by jointly fitting receiver functions and surface wave dispersion. *Geophysical Journal International*, **226**, 1645–1675. doi:10.1093/gji/ggab146
- Das, M.K., Agrawal, M., Gupta, R.K. & Gautam, J.L. (2019) Lithospheric seismic structure beneath two broadband station sites of the eastern part of Chhotanagpur Plateau: New constraints from receiver functions and dispersion curves. *Physics of the Earth and Planetary Interiors*, **287**, 51–64. doi:https://doi.org/10.1016/j.pepi.2019.01.004
- Gangopadhyay, A., Pulliam, J. & Sen, M.K. (2007) Waveform modelling of teleseismic S, Sp, SsPmP, and shear-coupled PL waves for crust- and upper-mantle velocity structure beneath Africa. *Geophysical Journal International*, **170**, 1210–1226. doi:10.1111/j.1365-246X.2007.03470.x

ACKNOWLEDEMENTS

Authors express their special thanks to the Centre for Development of Advanced Computing (C-DAC), Pune for providing the computation facilities in High Performance Computing (HPC) cluster of Param YUVA-II.

CONTACT

Mukesh Kumar Das
Observation Seismology Lab
Department of Applied Geophysics
IIT (ISM), Dhanbad
mukesh.17dr000318@agp.iitism.ac.in
Mob: +91-8873563108

Impact of extreme rainfall events on chemical weathering in a tropical river basin (Mahanadi river, India)

Rakesh Kumar Rout[1,*] and Gyana Ranjan Tripathy[1]

[1]Department of Earth and Climate Sciences, Indian Institute of Science Education and Research (IISER), Dr. Homi Bhabha Road, Pune-411008, India

(Email: *rout.rakesh@students.iiserpune.ac.in, grtripathy@iiserpune.ac.in)

INTRODUCTION:

Concentration-discharge relationship in a watershed provides quantitative assessment of seasonality in solute fluxes, weathering reactions and short-term weathering-climate linkage. These surface processes play a significant role in regulating atmospheric CO_2 budget and also, supply nutrients to the oceanic ecosystem. Time-series analyses of water chemistry of rivers are required to assess annual fluxes of these constituents and to constrain their controlling factors.

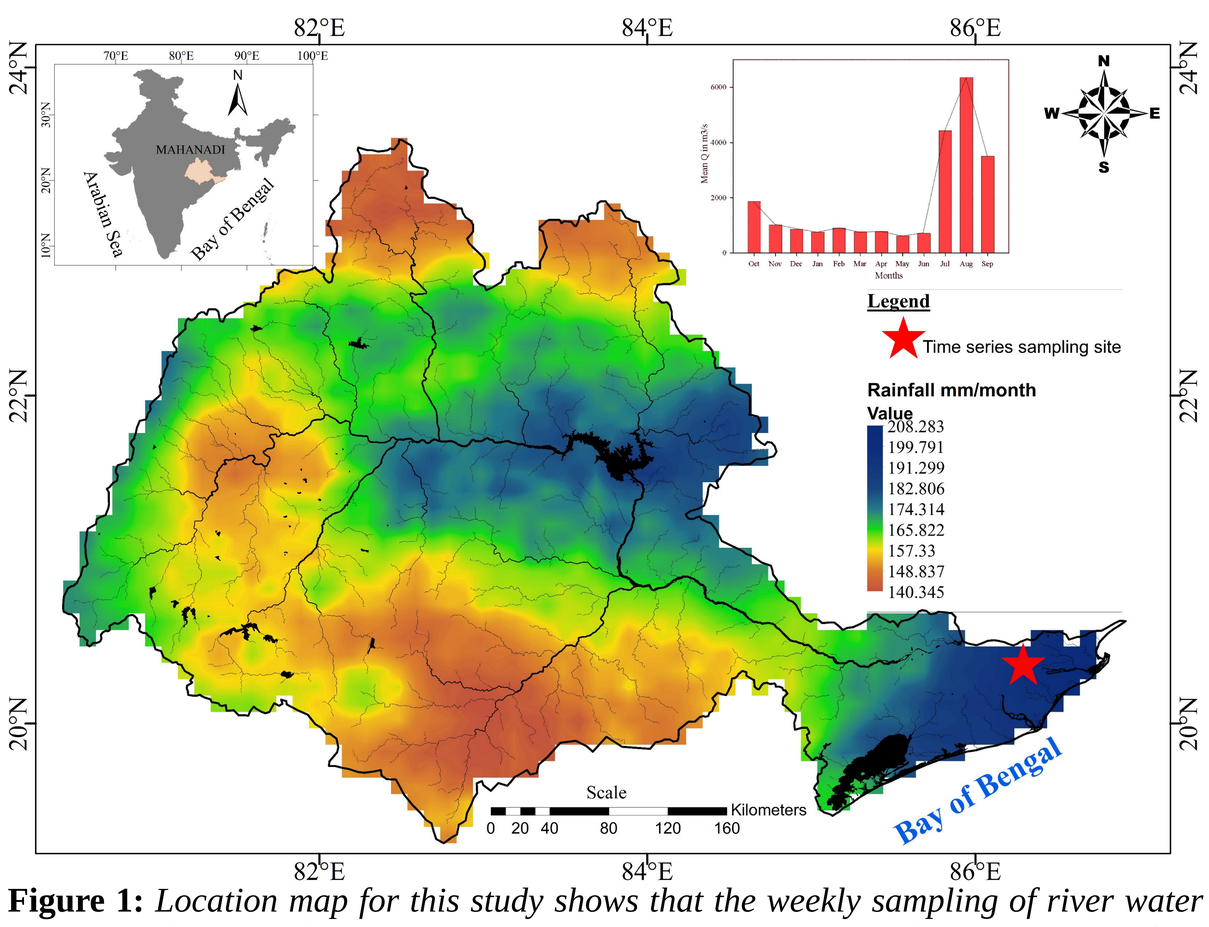

Figure 1: *Location map for this study shows that the weekly sampling of river water was done for one of the Mahanadi distributary (Paika river) for a duration of 15 months (11th August 2019 to 31st October 2020). The color contour in the figure reflects the average rainfall for the basin. Also, monthly average water discharge (1965-1970) at the Mahanadi outflow is shown in the figure inset (Date Source: https://nelson.wisc.edu/sage/data-and-models/riverdata).*

OBJECTIVE:

- To assess short-term climate sensitivity of the chemical weathering through time-series investigation of water chemistry of a tropical river.
- To assess seasonal change in mineral weathering intensity, if any, and its impact on solute load of rivers.
- To assess impact of cyclonic events on chemical weathering pattern of monsoon-fed river systems.

SAMPLES AND ANALYTICAL METHODS:

- Surface water samples were collected from a Mahanadi distributary (Paika river) for 15-months duration at weekly interval.
- These samples were analyzed for their major cations, anions and silica concentrations. Selected trace elements (Sr, Ba) concentrations were also measured.
- Real-time rainfall data during the studied period (https://indiawris.gov.in) were used to assess the weathering-climate interaction.

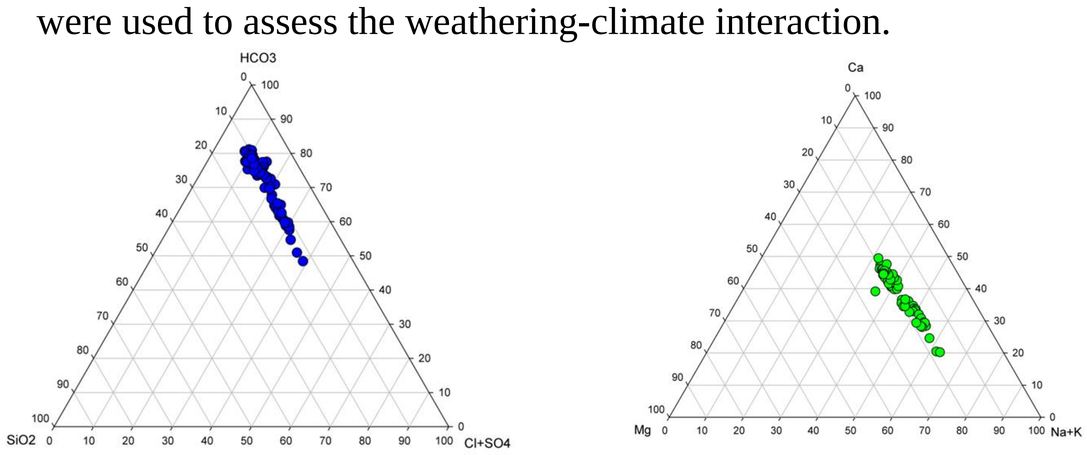

Figure 2: *Ternary plots show dominant solute contribution from the weathering of carbonate minerals to the basin.*

RESULTS:

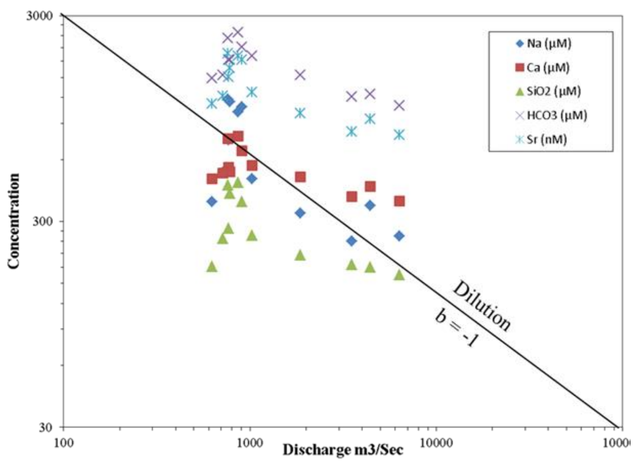

Figure 3: *Concentration-discharge relationship for the Mahanadi basin.*

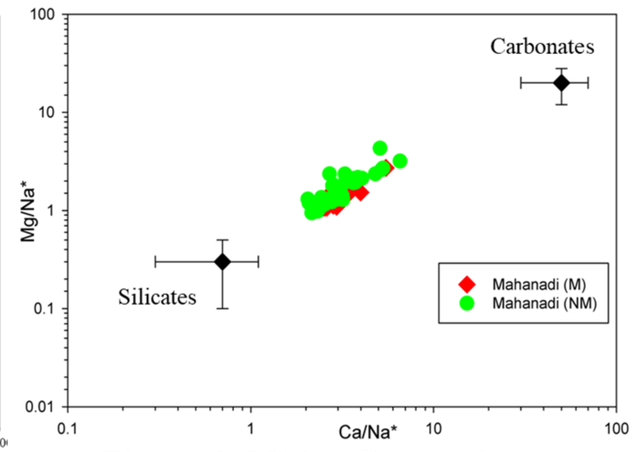

Figure 4: *Mixing diagram between Ca/Na* and Mg/Na* showing solute sources. Where M and NM represents monsoon and non-monsoon period, respectively.*

- Most of the elements show relatively lower concentrations during monsoon (by ~1.5 to 3 times) compared to that during the non-monsoon seasons.
- The total dissolved solid of this river varies between 90 and 305 mg/L, with an average value of 183 mg/L (n = 65).
- Mixing diagram show no significant seasonal change in relative solute contribution from the weathering of silicate/carbonate minerals.

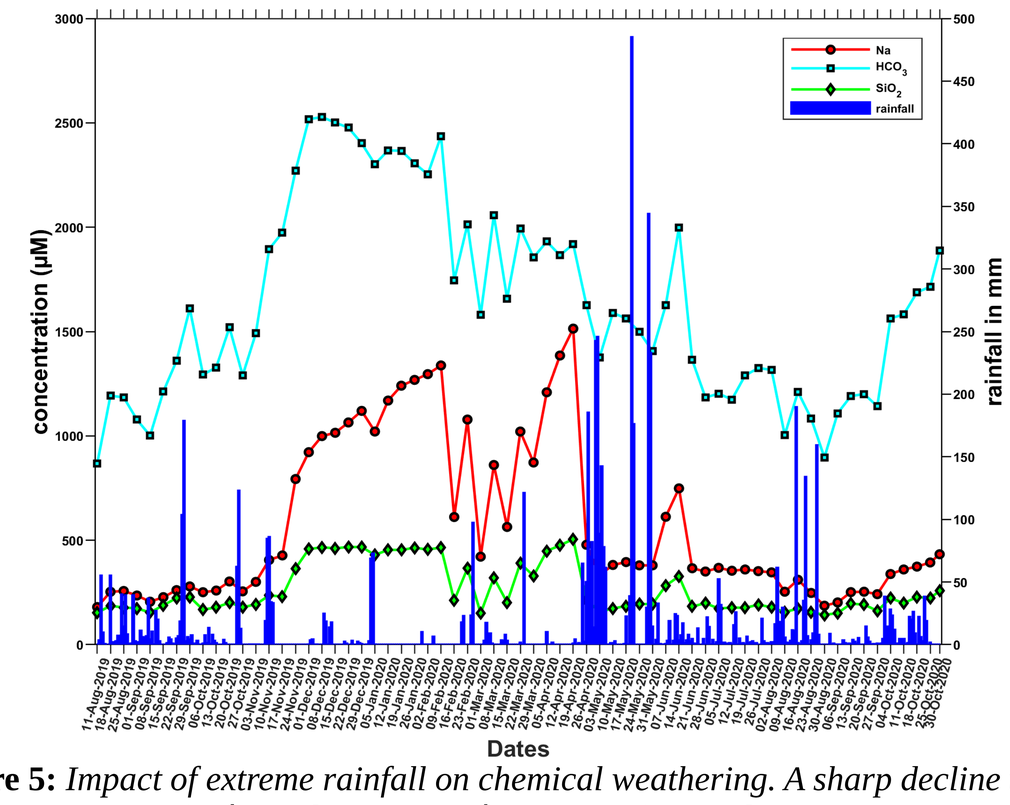

Figure 5: *Impact of extreme rainfall on chemical weathering. A sharp decline in major ion concentration (19th April 2020 to 24th May 2020) period.*

- A systematic decline in concentrations was noticed during a specific (19 April- 24 May) period in the pre-monsoon season which is synchronous to an extreme rainfall event occurred due to cyclonic disturbance occurred over the Bay of Bengal (BoB).
- Cyclonic rainfall influence the water chemistry by lowering elemental concentrations.
- These observation has been verified from the HYSPLIT backward trajectories model.

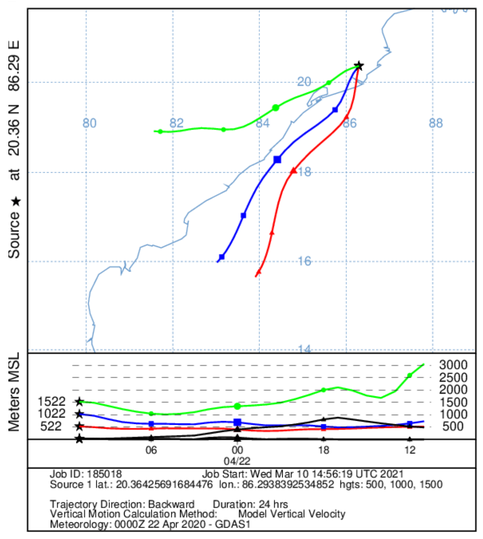

Figure 6: *HYSPLIT backward trajectories model shows moisture supply from the BoB during the cyclone.*

CONCLUSION:

- Seasonal changes in solute concentrations were observed.
- No signature of preferential change in silicate/carbonate weathering with water stages is observed.
- Strong control of weathering intensification during extreme rainfall event was observed.

Analysis of Seismic Attenuation Characteristics for Eastern Chotanagpur Plateau, India

Rashid Shams and Mohit Agrawal

Department of Applied Geophysics, Indian Institute of Technology (Indian School of Mines), Dhanbad, Jharkhand

Abstract

The Chotanagpur plateau is located at the northern periphery of the Singhbhum craton which manifests the north-eastern projection of Indian peninsula. Due to the presence of complex regional faults and the seismogenesis from the Himalayan collision zone in the north, the study region has suffered some moderate magnitude earthquakes, namely Hazaribagh (1868, M 5.0), Manbhum (1868, M 5.7), Bihar (1958), Ranchi (1963, M 5.0), Bankura (1969 M 5.7), Deogarh (2015, M 4.0), Sahibganj (2020, M 4.3), Deoghar (2020, M 4.1) and Jamshedpur (2020, M 3.9) along with some damaging historical major earthquakes viz. Bihar-Nepal border (1833, M 7.6), North of Bihar-Nepal Border (1934, M 8.1), Bihar (1988, M 6.8) and the most recent Gorkha Nepal earthquake (2015, M 7.8). In order to get insights into the seismicity, it is indispensable to study the attenuation characteristics of the region through estimation of Kappa (κ) and Coda-Q (Q_c) models for further stochastic simulation of ground motion. We use 139 seismic event records from sparsely located six broadband stations deployed in eastern part of Chotanagpur Plateau at Indian Institute of Technology, Dhanbad (IIT(ISM)), Sahibganj (SBG), Khunti (KNT), Bokaro (BOKR), Nirsa (NRS) and Peterwar (PTWR). Our results reveal that the average 'κ' value lies around 0.0364 for the region, which is dependent on the epicentral distance and independent of event's magnitude. The Q_c values are calculated for three-time windows of coda arrivals viz. 40 sec, 50 sec and 60 sec and are strongly dependent on frequencies. The calculated Q_c values are fitted using power law $Q_C = 281.09 f_c^{0.80}$, and is found to increase with increasing coda window. The extinction distance (L_E) indicates that the upper mantle is homogeneous and attenuation within the depth range 86 km to 119 km is comparatively less. Peak Normalized amplitude estimated for all six stations show decay with increase in distance. The lower Q_c values in the Bokaro region indicate presence of heat zones. The Q_c and 'n' values on comparison with Q_c model developed for other regions show that they lie between those of active and stable region implying moderate seismicity in the Eastern Chotanagpur Plateau region.

Objectives and Data used

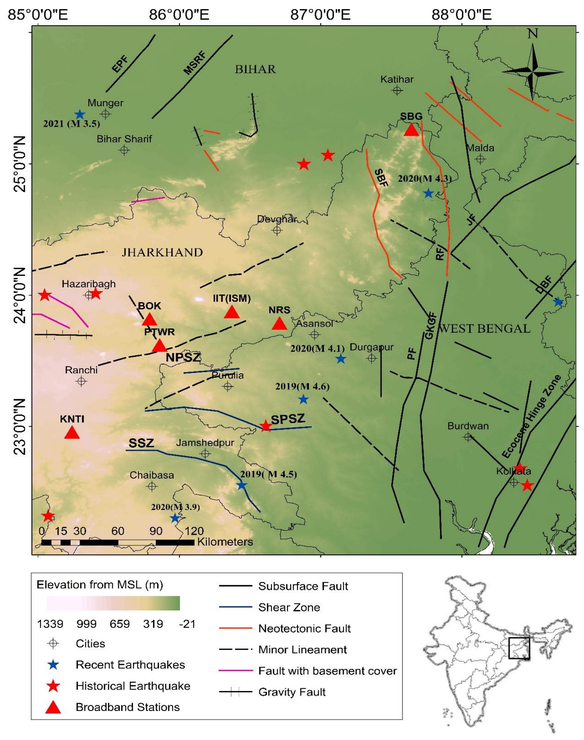

Study Area and Seismic Stations

- Development of **κ model** using the classical method by **Anderson and Hough (1984).**
- Estimation of **Coda-Q** using **Single backscattering model by Aki and Chouet (1975)**.
- **Seismic Broadband Stations**

1. IIT(ISM)
2. Sahibganj (SBG)
3. Khunti (KNTI)
4. Nirsa (NRS)
5. Bokaro (BOKR)
6. Peterwar (PTWR)

Methodology

Classical Method: Kappa Model

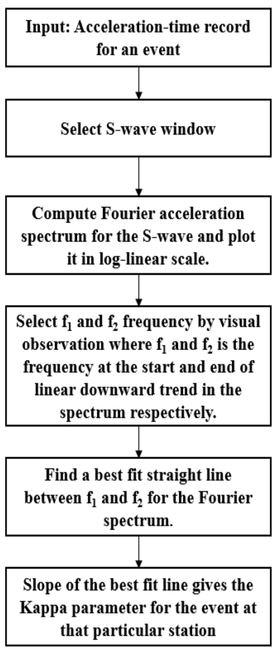

Single Backscattering Method

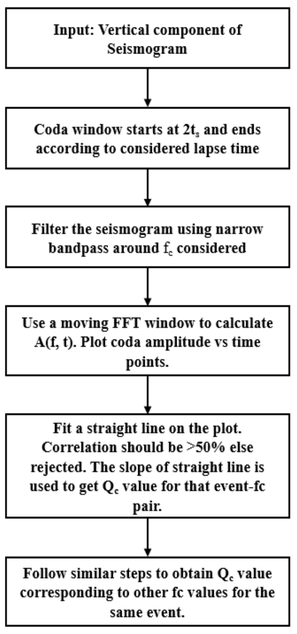

Results

Kappa Model for Vertical Component

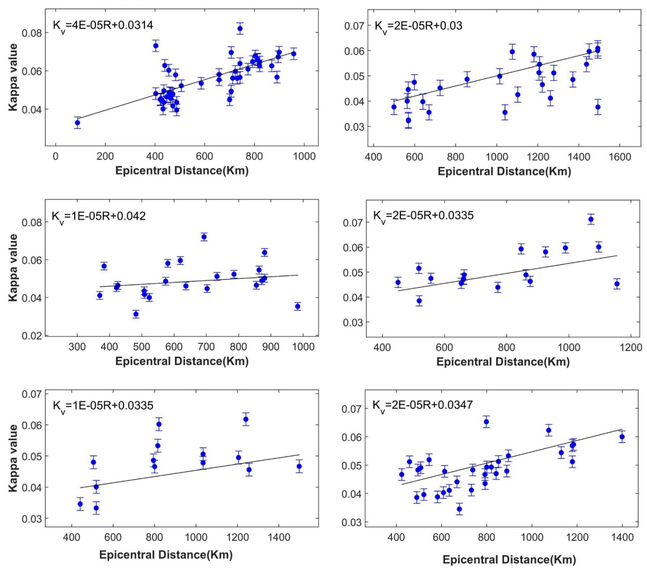

Coda-Q Model

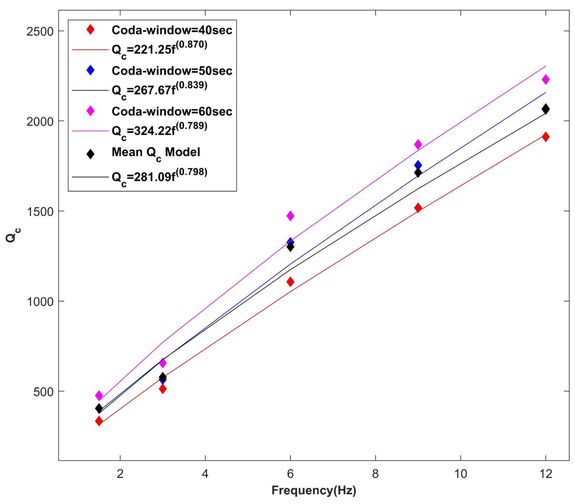

Variation of Coda-Q for each station

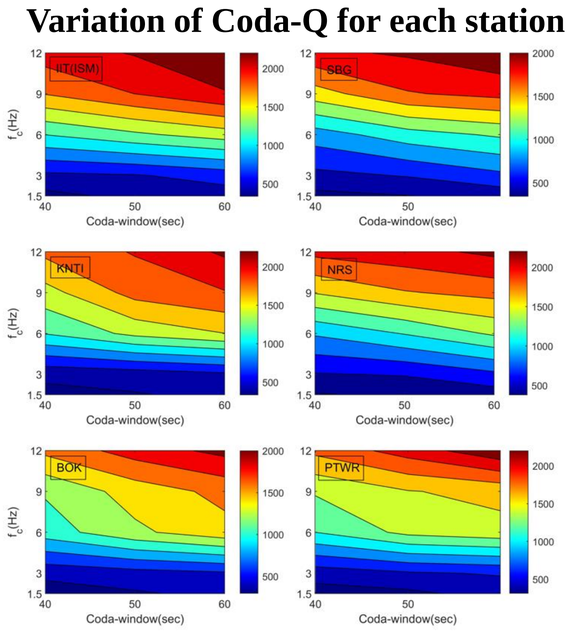

Extinction Distance (Le)

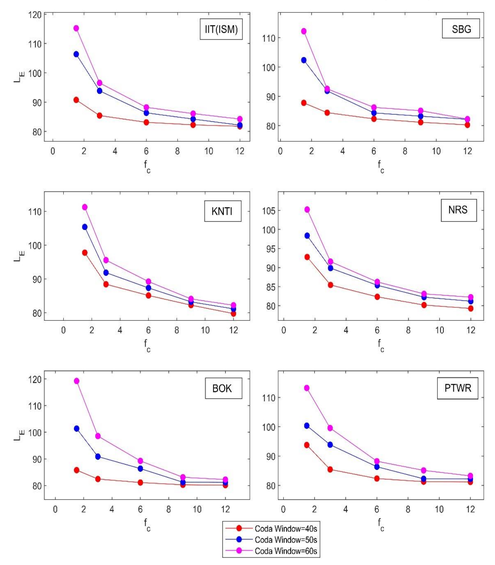

Comparison of Coda-Q Model

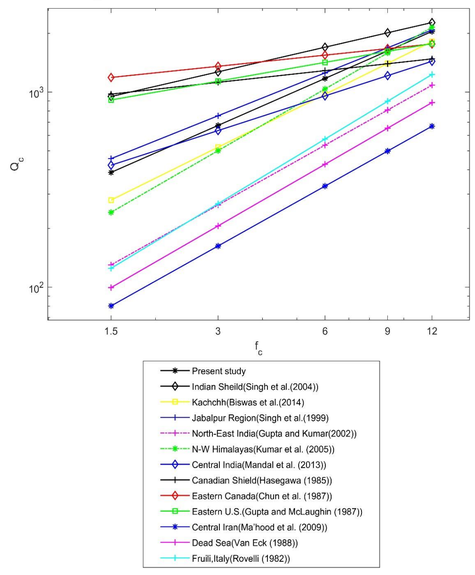

Conclusion

- The average value of **κo** is found to be **0.0364** for the ECNP region which is found comparable to other moderately seismic and stable regions.
- The **Coda-Q** estimated using data from six broadband stations viz. IIT(ISM), SBG, KNTI, NRS, BOK and PTWR at three Coda windows is found strongly dependent on frequency and obeying power law.
- The mean Q_c model estimated from analysis of all six stations for **40 sec, 50 sec and 60 sec Coda-window** are found the average Qc model for all windows and all stations is estimated as **Q_c=281.09$f_c^{0.80}$**
- The comparison of the developed Coda-Q model (Q_0>200 and n<0.90) suggests the **moderate seismicity** in the Eastern Chotanagpur Plateau Region.
- The extinction distance (L_E) indicates that the upper mantle is homogeneous and attenuation within the depth range 86 km to 119 km is comparatively less. Peak Normalized amplitude estimated for all six stations show decay with increase in distance.

References

- Anderson JG. Hough SE. (1984) A model for the shape of the Fourier amplitude spectrum of acceleration at high frequencies. Bull Seism Soc Am. 74:1969–1993.
- Aki K. Chouet B. (1975) Origin of Coda waves: source, attenuation and scattering effects. J Geophys Res 80:3322–3342.

Contact

Presenter- Rashid Shams,
Email- rashid98.20MT0321@agp.iitism.ac.in
IIT(ISM), Dhanbad.

Silicate versus carbonate rock weathering in Peninsular India: a study from the Kali watershed

Kumar Arun, Keshava Balakrishna and Harikripa Narayana Udayashankar

Department of Civil Engineering, Manipal Institute of Technology, Manipal Academy of Higher Education, Manipal-576104, India

ABSTRACT

Riverine chemistry of Kali watershed draining mixed silicate/carbonate lithologies was investigated to differentiate the impacts of silicate and carbonate rock weathering on river chemistry. Analysis of water samples for various Physico-chemical parameters and major ions were carried out for monsoon (July 2018), post-monsoon (December 2018) and pre-monsoon (May 2019) seasons. Stream water chemistry exhibits discrepancy in upstream, midstream, and downstream regions reflecting the slight variations in bedrock geology (weathering of silicate and carbonates rocks) and contributions from marine aerosols or other salts and anthropogenic sources. The catchment experiences intense chemical weathering on account of heavy rainfall, intense runoff during the monsoons. The estimated silicate and carbonate weathering rate is 41.3 t. km^{-2}. y^{-1} & 6.9 t. km^{-2}. y^{-1} in the river catchment. This could be attributed to intense rainfall-runoff and the nature of lithology, which mainly comprises greywackes, tonalitic gneiss and patches of limestone.

LOCATION & GEOLOGY

Study area map with sampling stations

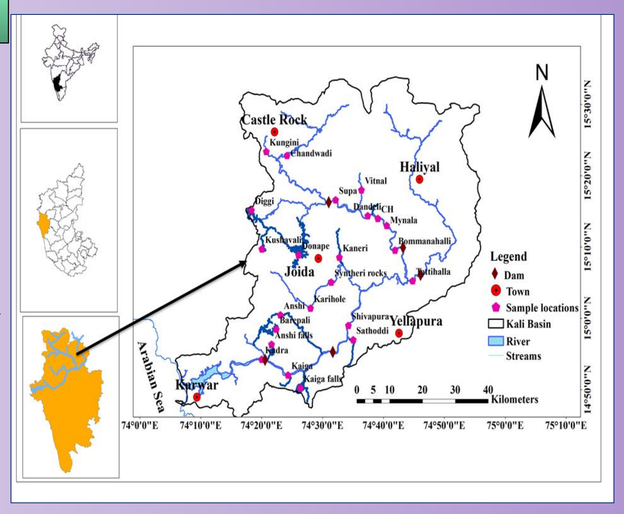

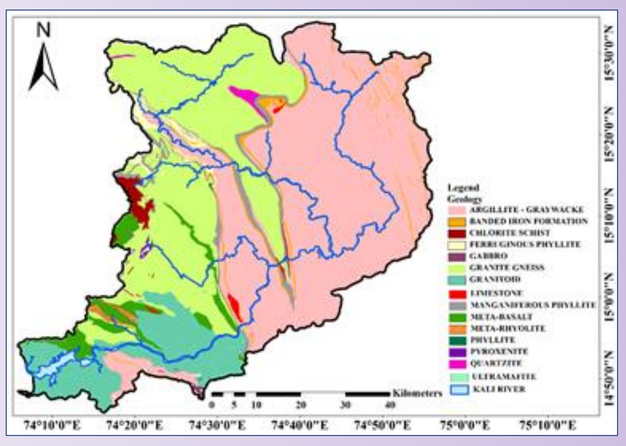

Lithological units of the study area (modified from Geological Survey of India).

METHODOLOGY

Seasonal collection of Surface water samples

↓

Onsite measurement of physical parameters (T, pH, DO, EC, TDS and alkalinity)

↓

Samples filtered through 0.22µm pore size Nucleopore polycarbonate filters

↓

Cations- Na^+, K^+, Mg^{2+},Ca^{2+} Using ion chromatography.

Silica UV-Vis-spectroscopy

RESULTS

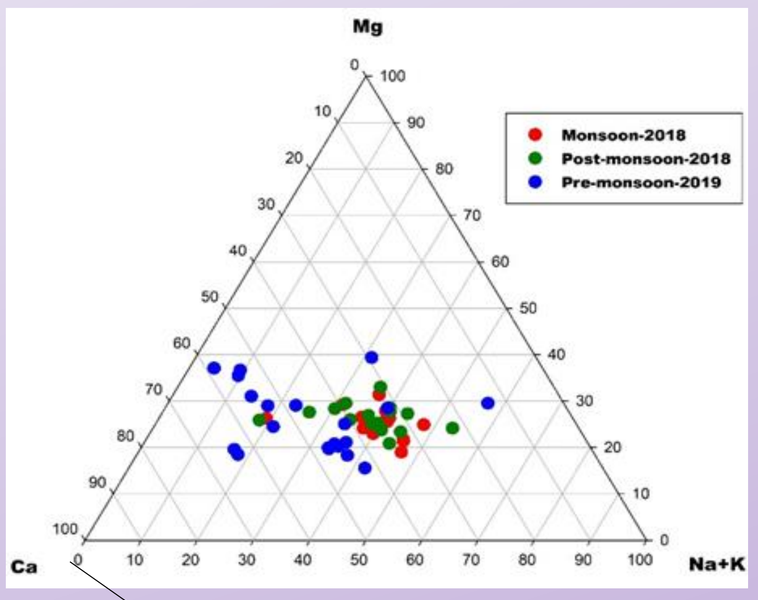

Ternary plots for cations

Sea salt corrected molar ratio of Ca/(Na+K) vs Mg/(Na+K)

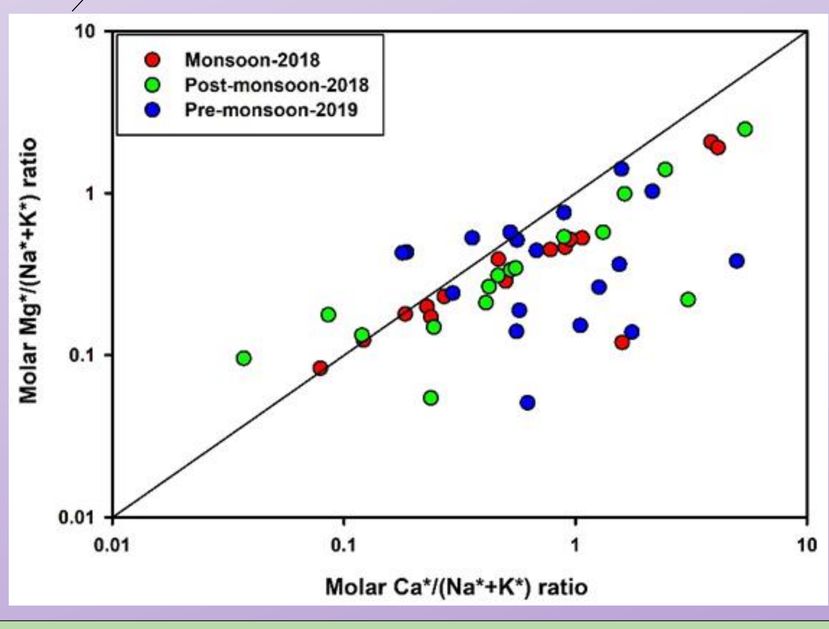

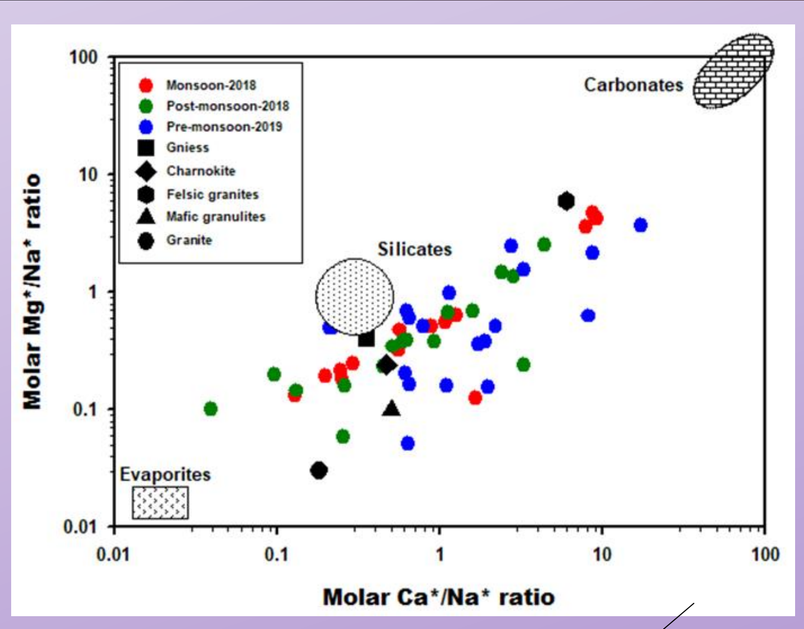

Sea salt corrected molar ratio of Ca/Na* vs Mg*/Na**

CONCLUSIONS

- Significant calcium enrichment in comparison with magnesium was observed for most of the samples in monsoon, post-monsoon, and pre-monsoon periods.
- The slope of the Mg/(Na+K) vs Ca/(Na+K) plot is lower in monsoon than pre-monsoon season, indicating the dissolution of trace calcite in the study area.
- Silicate rock weathering dominates majority of the study area, thus controlling the water chemistry.

ACKNOWLEDGEMENT

- Department of Science and Technology – INSPIRE fellowship.
- Ministry of Earth Sciences (MoES/CCR/Paleo-10/2015).
- MAHE for providing contingency grants and central instrumentation facilities for this study.

REFERENCES

- ✓ Bourgeon, G. (2001). A survey of soils and weathering patterns through land system mapping in the Western Ghats Region.
- ✓ Oliva, P., Dupré, B., Martin, F., & Viers, J. (2004). The role of trace minerals in chemical weathering in a high-elevation granitic watershed (Estibere, France): chemical and mineralogical evidence. *Geochimica et Cosmochimica Acta*, *68*(10), 2223-2243.
- ✓ bhukosh.gsi.gov.in

Comparison of Seismic Declustering Methods for Kishanganj (India)

Yehya RASOOL[1*] and Mohit Agrawal[2]

[1,2]Department of Applied Geophysics, Indian Institute of Technology (Indian School of Mines), Dhanbad, Jharkhand, India

*Email: rasool.yehya12@gmail.com; yehya.20mt0460@agp.iitism.ac.in

Abstract

This study appraises the seismicity of Kishanganj, a bordering district of Bihar, India and its adjoining region within a radius of 500 km by using several different Declustering methods. The methods are proposed by Gardner and Knopoff (1974), Zhuang et al. (2002) or stochastic declustering algorithm and Reasenberg (1985). From the results, it is clear that each algorithm has different influence on raw catalog, which may, in turn, provoke influences on seismic hazard analysis. The Gardner and Knopoff (1974) algorithm, which is a window based method, yields only 19% of clustered events and removes 81% of total events, thus fails to consider all the background events. This algorithm also spots the foreshocks and aftershocks with a greater shaking intensity than their analogous parent events. This may be due to the application of window method in Gardner and Knopoff (1974) algorithm. The Reasenberg (1974) algorithm, which is a clustering based method, removes 13.7% of the total events. This algorithm removes relatively less amount of foreshocks and aftershocks. The Zhuang et al. (2002) proposed an algorithm, based on Epidemic Type Aftershock Sequence (ETAS) Model (Ogata, 1988 and Ogata, 1998) also known as stochastic declustering, which removes 33% of offspring events. This algorithm amalgamates the parametric maximum likelihood for clustering structures by employing space-time ETAS model and the non-parametric estimate of parent seismicity also known by variable weighted kernel estimate. The clustering and window methods are easier to execute than stochastic declustering. From this study, it is clear that clustering method is suitable to our study region for declustering and seismic hazard analysis.

Introduction

- In our investigation, we have used three most popular declustering approaches in order to understand the comparison between them: i). Window based method (i.e. Gardner and Knopoff, 1994). ii). Clustering method (i.e. Reasenberg, 1985) and iii). Stochastic method (i.e. ETAS model). The widow based method was introduced by Gardner and Knopoff (1974), assembles events according to space and time windows.

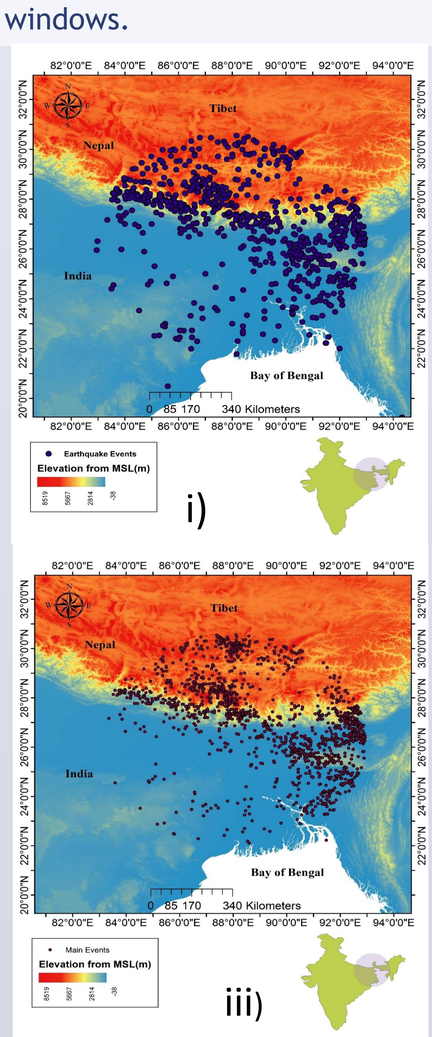

Figure captions:
Distribution of epicenters for declustered catalogs by using:
i). Gardner and Knopoff (1974) algorithm
ii). Reasenberg(1984) algorithm.
iii). ETAS model algorithm

Methodology

- Three famous algorithms:
- Gardner and Knopoff (1974)

$$\mathrm{Log_{10}T} = \begin{cases} 0.032\,\mathrm{M} + 2.7389\,, \text{for } \mathrm{M} \geq 6.5 \\ 0.5409\,\mathrm{M} - 0.547, \text{ otherwise} \end{cases}$$

$$\mathrm{Log_{10}L} = 0.1238\,\mathrm{M} + 0.983$$

- Reasenberg (1984)

$$P(\aleph[t, t+\tau]) = n) = \frac{e^{-\lambda(t)\tau}}{n!}[\lambda(t)\tau]^n$$

$$\lambda(t) = k(t+c)^{-p}$$

Where 'L (Km)' and 'T (days)' are the location and time windows respectively and 'M' is the moment magnitude of earthquake event

'ℵ' corresponds to the process that estimates the number of independent events occurring within the above mentioned time interval and p, c and k corresponding the positive constants representing the parameters of Omori's law.

- ETAS model (Zhuang et al., 2002)

$$\lambda(t, x, y, M|\mathcal{H}_t) = \lambda(t, x, y, \mathcal{H}_t)\ \mathrm{J(M)}$$

$$\rho_j = \sum_{i<j} \rho_{ij}$$

$$\rho_{ij} = \begin{cases} \frac{\mathfrak{z}(t_i, x_{i,y_i})}{\lambda((t_i, x_{i,y_i}|\mathcal{H}_t j)} & \text{for j > i} \\ 0, \quad otherwise \end{cases}$$

$$\Phi j = 1 - \rho_j$$

Where, λ is the conditional intensity of antiquity of observation $\mathcal{H}_t$up to time't', and μ, k(M), g, f and J are the background events, expected number of offspring events, Probability distribution function, spatial distribution of the offspring events and magnitude distribution function respectively.

Results

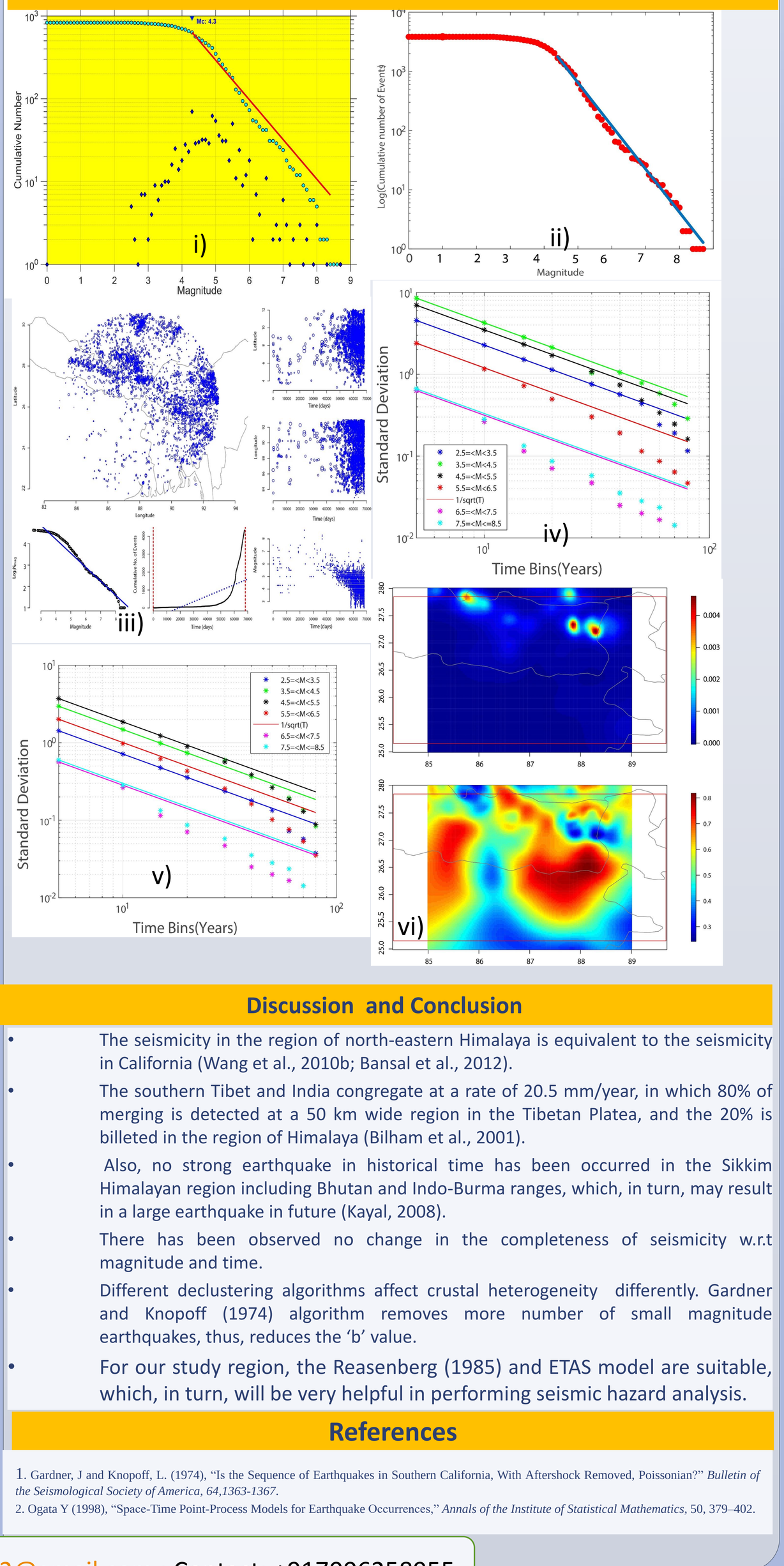

Discussion and Conclusion

- The seismicity in the region of north-eastern Himalaya is equivalent to the seismicity in California (Wang et al., 2010b; Bansal et al., 2012).
- The southern Tibet and India congregate at a rate of 20.5 mm/year, in which 80% of merging is detected at a 50 km wide region in the Tibetan Platea, and the 20% is billeted in the region of Himalaya (Bilham et al., 2001).
- Also, no strong earthquake in historical time has been occurred in the Sikkim Himalayan region including Bhutan and Indo-Burma ranges, which, in turn, may result in a large earthquake in future (Kayal, 2008).
- There has been observed no change in the completeness of seismicity w.r.t magnitude and time.
- Different declustering algorithms affect crustal heterogeneity differently. Gardner and Knopoff (1974) algorithm removes more number of small magnitude earthquakes, thus, reduces the 'b' value.
- For our study region, the Reasenberg (1985) and ETAS model are suitable, which, in turn, will be very helpful in performing seismic hazard analysis.

References

1. Gardner, J and Knopoff, L. (1974), "Is the Sequence of Earthquakes in Southern California, With Aftershock Removed, Poissonian?" *Bulletin of the Seismological Society of America, 64,1363-1367.*

2. Ogata Y (1998), "Space-Time Point-Process Models for Earthquake Occurrences," *Annals of the Institute of Statistical Mathematics*, 50, 379–402.

Presenter: Yehya Rasool; rasool.yehya12@gmail.com ; Contact: +917006258955

Comparison of the LST, NDVI, and NDBI between the old Ahmedabad city and the new Ahmedabad city using the LANDSAT-8 satellite

Divyakumar A. Kotia, Akhil S. Nair, Tejas Turakhia, Rajesh Iyer
St. Xavier's College (Autonomous), Ahmedabad-380009, Gujarat, India

AIM

Older parts of the cities are used to be more densed & tightly packed because in the older times most of the infrastructures used to be in a small allotted area and the outskirts of the city used to be kept reserved for the vegetation activities. Now due to urbanization, cities are getting bigger but still the older parts are more densed as compared to the newly developed parts of the cities. In this study, a comparison between the Old Ahmedabad city and the New Ahmedabad city is made in terms of LST, NDVI, and NDBI. These are obtained by using the data derived from the LANDSAT-8 OLI and TIRS. In this study mean values of LST, NDVI, and NDBI for different seasons of the year 2020 are considered for both parts of the city.

INTRODUCTION

- **Land surface temperature (LST)** is the radiative skin temperature of the land derived from solar radiation

$$T_s = \frac{BT}{\left\{1 + \left[\left(\lambda BT/\rho\right) ln\varepsilon_\lambda\right]\right\}}$$

- **Normalized Difference Vegetation Index (NDVI)** quantifies vegetation by measuring the difference between near-infrared (which vegetation strongly reflects) and red light (which vegetation absorbs).

$$NDVI = \frac{NIR - Red}{NIR + Red}$$

- **Normalized Difference Vegetation Index (NDBI)** quantifies urban areas where there is typically a higher reflectance in the shortwave-infrared (SWIR) region, compared to the near-infrared (NIR) region.

$$NDBI = \frac{SWIR - NIR}{SWIR + NIR}$$

METHODOLOGY

- Google earth engine was used to compute the values of LST, NDVI & NDBI in the .csv form by following the steps as mentioned in fig. (1). The details of the data obtained is mentioned in the Table (1).
- Pixel wise correlation of LST with NDVI & NDBI was obtained by using the Q-GIS.

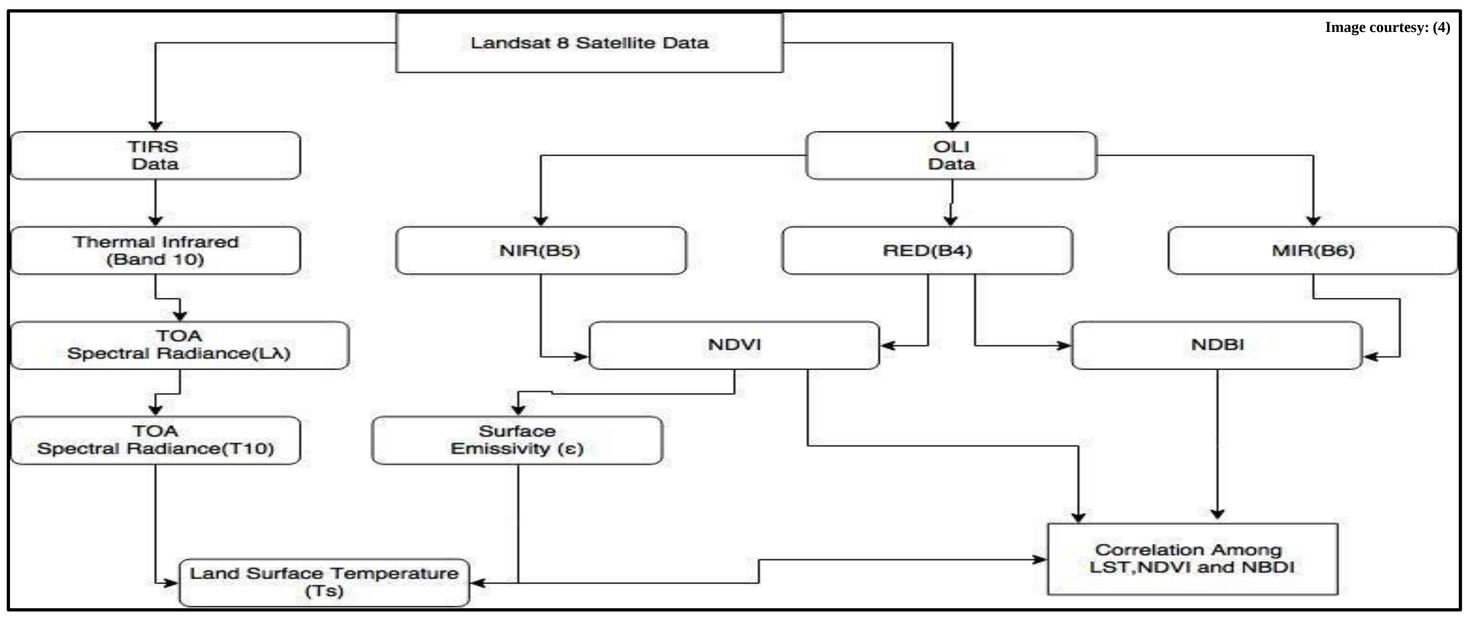

Fig. (1)

Satellite	Image collection	Sensor	Bands	Spatial resolution
LANDSAT-8	USGS Landsat 8 Surface Reflectance Tier 1	OLI/TIRS	Bands 4 (NIR), 5 (Red), 6 (SWIR) & 10(TIR)	30 m

Table (1) Details of the satellite data

RESULTS

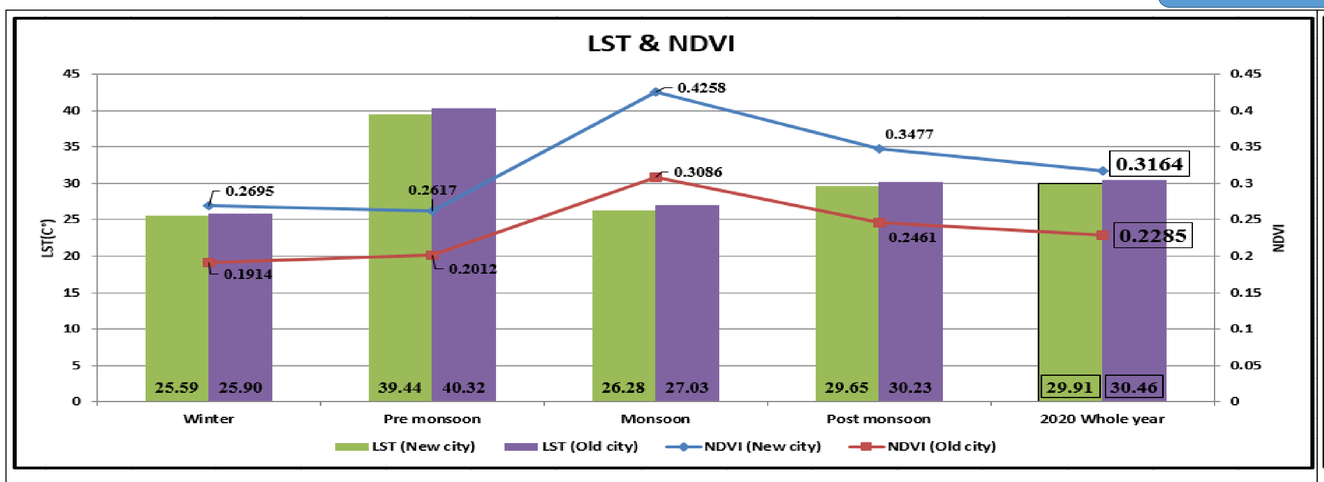

Fig. (2)

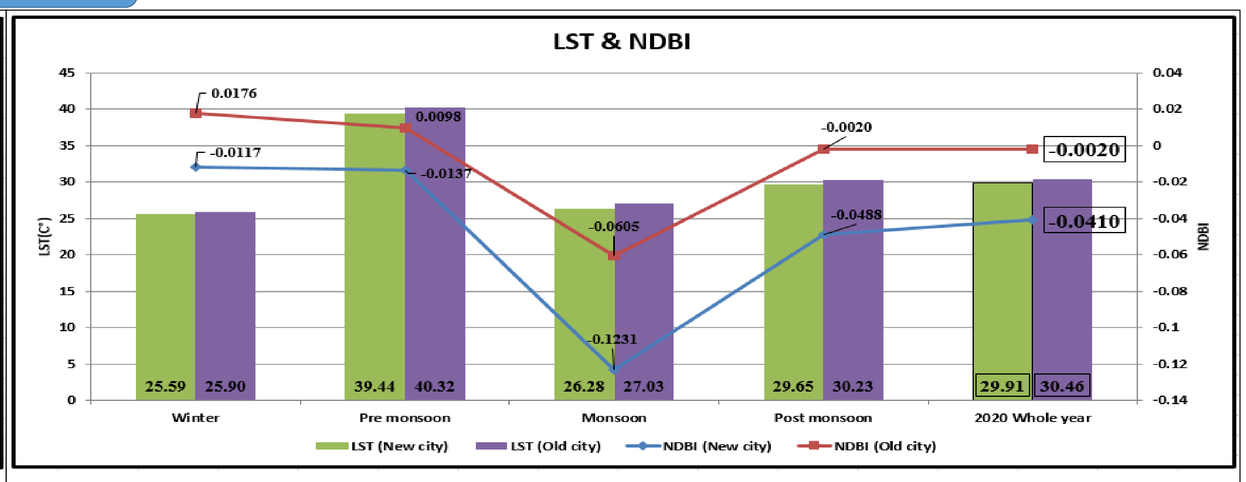

Fig. (3)

Seasons	LST (°C)	NDVI	NDBI
Winter	0.31 (1.20 %)	-0.08 (-28.98 %)	0.03 (250.78 %)
Pre monsoon	0.88 (2.24 %)	-0.06 (-23.12 %)	0.02 (171.67 %)
Monsoon	0.74 (2.82 %)	-0.12 (-27.52 %)	0.06 (50.81 %)
Post monsoon	0.58 (1.94 %)	-0.10 (-29.22 %)	0.05 (95.92 %)
2020	**0.55 (1.81 %)**	**-0.09 (-27.78 %)**	**0.04 (95.21 %)**

Table (2) – Comparison (Difference) of Old city with the New city

Correlations (r)

	Max (New city, Old city)	Min (New city, Old city)
LST-NDVI	Monsoon (-0.52, -0.58)	Premonsoon (-0.13), Winter (-0.16)
LST-NDBI	Post monsoon (0.67, 0.72)	Winter (0.57, 0.58)

- The correlation of LST with NDVI & NDBI was found out to be more for the old Ahmedabad city as compared to the new city.

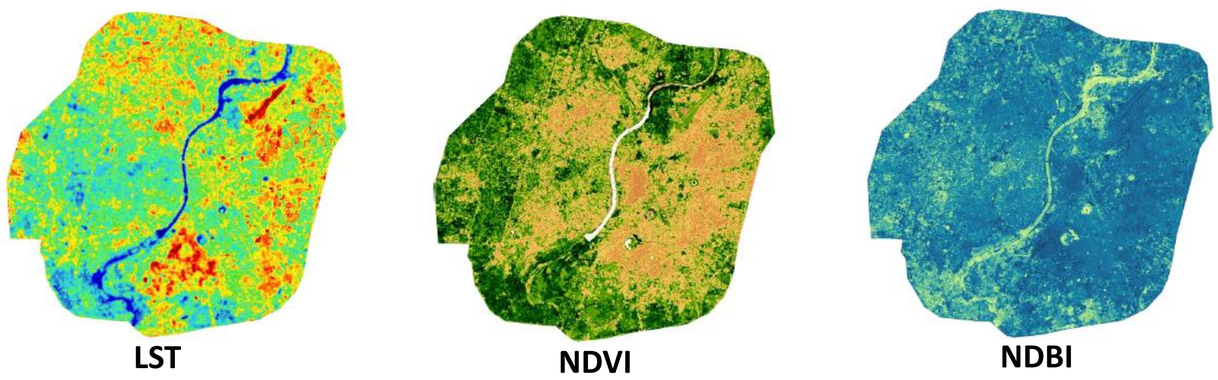

Fig. (4) Maps of LST, NDVI & NDBI

CONCLUSION

- **From this study it can be known that the old Ahmedabad city (Eastern side of the river) is having more LST than the new city (Western side of the river) due to its fewer vegetation areas and highly dense built-up areas. This kind of trend was seen for all the seasons of the year 2020. The trend observed in this study can be implied for some other cities also.**

REFERENCES

1. Algorithm for Automated Mapping of Land Surface Temperature Using LANDSAT 8 Satellite Data – Ugur Avdan and Gordana Jovanovska
2. Subhanil Guha, Himanshu Govil, Prabhat Diwan, "Analytical study of seasonal variability in land surface temperature with normalized difference vegetation index, normalized difference water index, normalized difference built-up index, and normalized multiband drought index," J. Appl. Remote Sens. 13(2), 024518 (2019), doi: 10.1117/1.JRS.13.024518.
3. Ashwani kumar Agnihotri, Anurag Ohri, Sachin Mishra, "Remote sensing Based Assessment of Urban Heat Island From TIRS data -A case study of Varanasi city, India"
4. Advanced remote sensing terrestrial information extraction and applications by Liang, Shunlin Wang, Jindi

ACKNOWLEDGEMENT: We would like to express our gratitude to Physical Research Laboratory (PRL) for providing an opportunity to present our work. Also, we are thankful to St. Xavier's college, Ahmedabad and we are also very grateful to our parents & friends for their support and encouragement.